Check for updates

ADVANCING EARTH AND SPACE SCIENCE

JGR Oceans

RESEARCH ARTICLE
10.1029/2022JC018624

**Key Points:**

- A seamless characterization of New Zealand's ocean circulation is achieved from a high-resolution, 28 yr model simulation
- Interannual variability in boundary current transport and upper ocean heat content (UOHC) show large-scale correlations over the NZ oceanic region
- Sea Surface Height and UOHC co-vary indicating large-scale ocean currents and mesoscale eddies drive UOHC changes

**Correspondence to:**
C. Kerry,
c.kerry@unsw.edu.au

**Citation:**
Kerry, C., Roughan, M., & De Souza, J. (2023). Characterizing the variability of boundary currents and ocean heat content around New Zealand using a multi-decadal high-resolution regional ocean model. *Journal of Geophysical Research: Oceans*, *128*, e2022JC018624. https://doi.org/10.1029/2022JC018624

Received 22 MAR 2022
Accepted 31 MAR 2023

© 2023. The Authors.
This is an open access article under the terms of the Creative Commons Attribution-NonCommercial-NoDerivs License, which permits use and distribution in any medium, provided the original work is properly cited, the use is non-commercial and no modifications or adaptations are made.

# Characterizing the Variability of Boundary Currents and Ocean Heat Content Around New Zealand Using a Multi-Decadal High-Resolution Regional Ocean Model

**Colette Kerry[1], Moninya Roughan[1], and Joao De Souza[2]**

[1]Coastal and Regional Oceanography Lab, School of Biological, Earth and Environmental Sciences, UNSW Australia, Sydney, NSW, Australia, [2]MetOcean Solutions, a Division of Meteorological Service of New Zealand, Raglan, New Zealand

**Abstract** New Zealand is located in the southwest Pacific Ocean and is surrounded by a complex system of boundary currents that vary on a variety of time scales, with important impacts on weather, primary productivity, and fisheries. While various observational and modeling studies have shed light on many of the characteristics of New Zealand's ocean circulation, this study provides a comprehensive, quantitative, seamless, 3-dimensional characterization of the region's boundary current circulation and ocean heat content. We use a 28 yr long hydrodynamic model simulation that accurately represents the mean and variability of the ocean circulation to characterize and quantify the temporal and spatial variability across the region. We show that low-frequency variability in boundary current transport and upper ocean heat content are correlated over the entire New Zealand oceanic region. Oceanic eddies dominate heat content variability at intra-annual scales in the northeast of the region, while on the west and southeast coasts heat content varies predominantly at interannual scales controlled by large-scale changes in the subtropical and sub-Antarctic fronts. The model shows a significant downstream strengthening and deepening of the boundary currents off northeast New Zealand which, if confirmed by observations, could suggest a significant new understanding of this Western Boundary Current system. This study presents a region-wide characterization of the temporal and spatial variability of ocean currents and heat content, and their interconnections, providing a vital basis for understanding climate change impacts and the increasing occurrence of marine heatwaves.

**Plain Language Summary** The ocean currents around New Zealand are complex and have both tropical and sub-Antarctic origins. The currents vary in space and time on a variety of scales, and impact weather, primary productivity, and fisheries. Here, we use an ocean model to represent the circulation around New Zealand over a 28 yr period. This representation allows us to study the spatial and temporal variability of ocean currents and heat content across New Zealand's oceanic region. Increased understanding of the variability and interconnections of ocean currents and heat content is key to predicting ocean temperature extremes and the response of NZ's oceans to global environmental change.

## 1. Introduction

New Zealand (NZ) is located in the western South Pacific Ocean and is influenced by and has an influence on both the South Pacific Subtropical Gyre and Southern Ocean circumpolar fronts (Chiswell et al., 2015; Saunders et al., 1999; Tomczak & Godfrey, 1994), resulting in a complex system of boundary currents. The country is comprised of a number of islands; the two main islands lie in the north to south direction and the complex topography contributes to complexities in shelf and boundary current circulation. Various studies have shed light on some of the characteristics of NZ's ocean circulation (e.g., Chandler et al., 2019; Chiswell, 1996, 2005; Santana et al., 2021; Stanton, 1995; Sutton, 2003), including review papers by Chiswell et al. (2015) and Stevens et al. (2019). A comprehensive observational view of the currents along NZ's eastern margin is presented in Fernandez et al. (2018) using both altimetry and in situ observations. Bowen et al. (2017) and Sutton and Bowen (2019) described the region's circulation in terms of temperature change, temperature trends, and links to air temperatures in the region. While NZ's currents have been investigated numerous times in the past, individually and collectively from observations and simulations, this study aims to strengthen the understanding of NZ's ocean circulation by providing a seamless, region-wide, 3-dimensional characterization of the region's boundary current circulation and ocean heat content across three decades. We use a high-resolution (5 km), three-dimensional, 28 yr hindcast, that realistically represents the ocean circulation and its variability around NZ

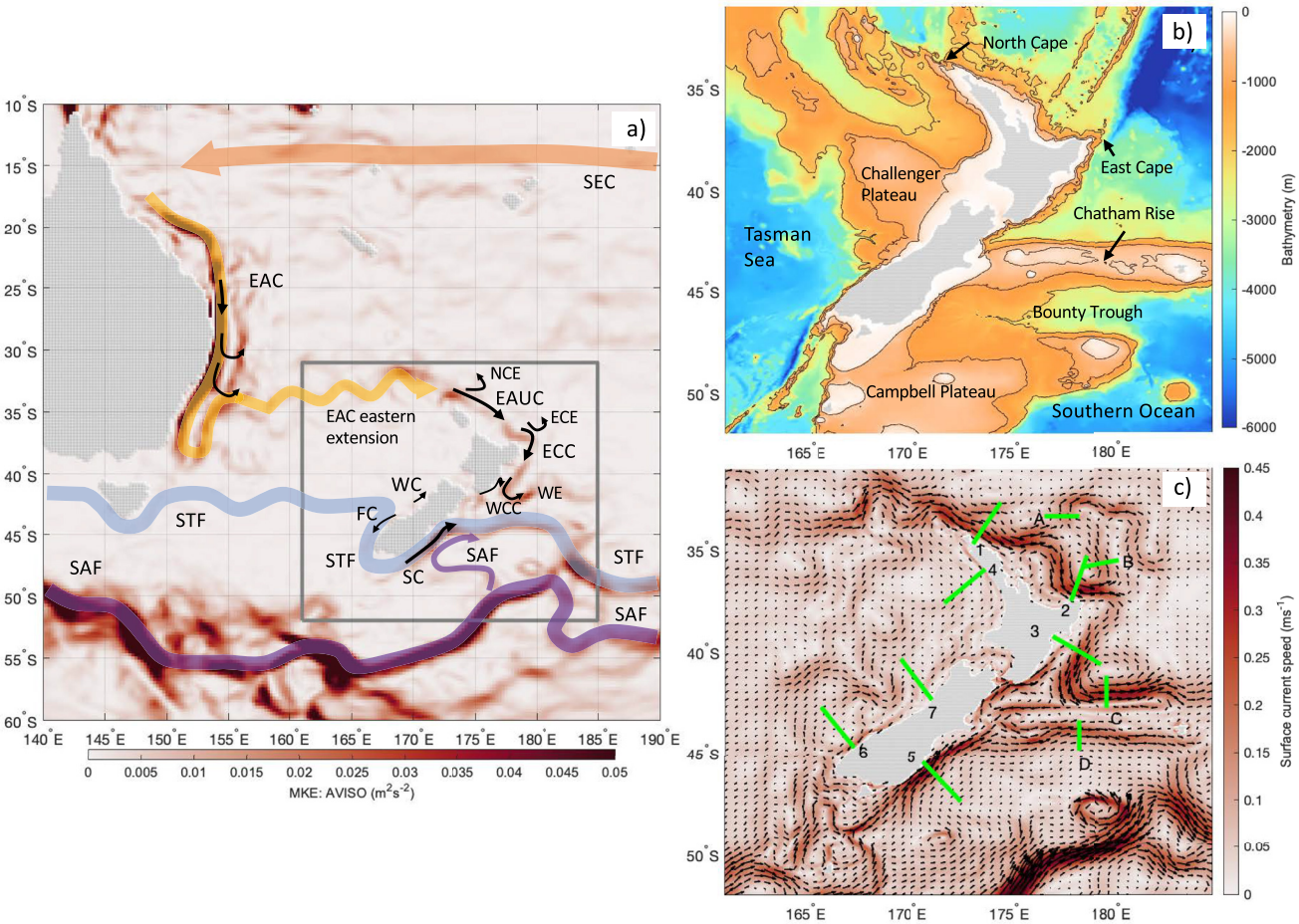


**Figure 1.** Mean Kinetic Energy (MKE) over the southwest Pacific with a schematic of major ocean currents and fronts, and showing model domain (a). Current, eddy, and front names are defined in Section 2. Model bathymetry with 400, 1,000, 2,000 m contours and bathymetric features labeled (b). Mean surface current speed and velocity vectors from daily-average output from the Moana Ocean Hindcast (c). Sections for velocity cross-sections and transport calculations are shown: 1. East Auckland Current (EAUC), 2. EAUC South, 3. East Cape Current (ECC), 4. West coast of North Island, 5. Southland Current (SC), 6. Fiordland Current (FC), 7. Westland Current (WC), A. North Cape Separation, B. East Cape Separation, C. Wairarapa Separation, D. Southland Current Separation.

(Azevedo Correia de Souza et al., 2022) to characterize the depth structure of NZ's boundary currents and the intra-annual, seasonal and inter-annual variability of the currents and heat content across the region.

To describe the circulation around NZ we must first understand its position in the basin-scale wind-driven circulation, so we begin by presenting a review of NZ's ocean circulation (shown in Figure 1). We then use the model output to describe the region's eddy variability and the three-dimensional structure and variability of the major boundary currents. We show that low frequency (periods >450 days) variability in boundary current transport and upper ocean heat content (UOHC) show large-scale correlations over the entire NZ oceanic region. Our results reveal that Sea Surface Height (SSH) and UOHC vary with similar spatial structure at both low frequency (annual and inter-annual) and intra-annual frequencies, indicating that both large-scale adjustments, boundary current, and eddy-related transport drive UOHC to varying degrees across the region.

This study's strength lies in the long-term, high-resolution, 3-dimensional, hindcast of the entire NZ region, which allows the relationships between boundary currents and ocean heat content to be investigated using a seamless approach across the region. Specifically, the high-resolution allows the complex coastal boundary currents and temperature variability to be resolved. Using this model we provide a basis for understanding the inter-connections between large-scale (region-wide) changes, boundary current transport, and ocean heat content, and demonstrate the temporal and spatial scales of variability. This characterization represents a crucial first step



21699291, 2023, 4, Downloaded from https://agupubs.onlinelibrary.wiley.com/doi/10.1029/2022JC018624 by University of New South Wales, Wiley Online Library on [16/10/2023]. See the Terms and Conditions (https://onlinelibrary.wiley.com/terms-and-conditions) on Wiley Online Library for rules of use; OA articles are governed by the applicable Creative Commons License

toward understanding how NZ's ocean might respond to global warming and toward predicting the likelihood, severity, and timing of ocean temperature extremes. The understanding gained by this study, combined with advanced modeling tools, has been used to study the dominant drivers of extended periods of anomalously warm ocean temperatures (marine heatwaves, Hobday et al., 2016) in NZ's shelf seas (Kerry et al., 2022). We focus on characterizing the mean and variability of boundary currents and UOHC around NZ at intra-annual, seasonal, and intra-annual timescales; future studies could use the hindcast to look at long-term trends and to diagnose the dynamical drivers of boundary current and UOHC variability across the region.

## 2. New Zealand's Ocean Circulation

### 2.1. The South Pacific Subtropical Gyre

In the South Pacific subtropical gyre, the South Equatorial Current is the northern link of the gyre which flows westward in a broad band centered at approximately 17°S transporting water across the equatorial Pacific to eastern Australia (Ganachaud et al., 2014; Reid, 1986). The required poleward return flow occurs in an intense Western Boundary Current (WBC) on the western margin of the ocean basin, the East Australian Current (EAC), which advects warm oligotrophic water and biota polewards along the east coast of Australia (Kerry & Roughan, 2020; Oke et al., 2019; Ridgway & Godfrey, 1994; Roughan & Middleton, 2004; Suthers et al., 2011).

Along the coast of southeastern Australia the EAC typically flows as a continuous, poleward-flowing current adjacent to the coast from ∼27°–30°S (Archer et al., 2017; Sloyan et al., 2016), before separating from the coast between 31° and 34°S (Cetina Heredia et al., 2014; Kerry & Roughan, 2020; Ridgway & Dunn, 2003) forming a complex field of eddies. The transient, eddy dominated flow between Australia and NZ has traditionally been referred to as the Tasman Front, but more recently has been referred to as the "EAC eastern extension" (Oke, Pilo, Ridgway, Kiss, & Rykova, 2019; Oke et al., 2019). Separation of the EAC results from a combination of intrinsic instabilities in the EAC jet and westward propagating Rossby waves (J. Li et al., 2021; Kerry & Roughan, 2020; Wilkin & Zhang, 2007), with bathymetric features around NZ playing a key role in controlling the EAC separation latitude and the mean location of the EAC eastern extension (Bull et al., 2018). Previous studies have also suggested that wind stress curl plays a role in the partial separation of the EAC (Bostock et al., 2006; Oliver & Holbrook, 2014; Tilburg et al., 2001). On average about 2/3 of the poleward flowing EAC turns eastward to feed the EAC eastern extension and 1/3 continues southward of the separation zone (Kerry & Roughan, 2020; Ridgway & Godfrey, 1997; Ypma et al., 2016).

### 2.2. North Island Boundary Currents

The region of elevated eddy variability associated with the EAC eddy field in the Tasman Sea extends along the path of the EAC eastern extension to the northern tip of NZ (Qiu & Chen, 2004), and this eddy train partially feeds the inflow of the East Auckland Current (EAUC) at the northern tip of New Zealand (Chiswell et al., 2015; Oke et al., 2019; Tilburg et al., 2001; Figure 1). A system of semi-permanent eddies are prominent features of the circulation along the east coast of the NZ's North Island, associated with the EAUC and East Cape Current (ECC) systems (e.g., Fernandez et al., 2018; Roemmich & Sutton, 1998; Stevens et al., 2019; Tilburg et al., 2001); the North Cape Eddy (NCE), the East Cape Eddy (ECE), the Wairarapa Eddy (WE) and the (smaller and weaker) Hikurangi Eddy. Chiswell (2005) suggested that, rather than describing the system south of East Cape as a series of semi-permanent eddies (that are present in the long-term SSH mean), the system is better described as a sequence of eddies shed near East Cape that propagate down the coast. To the north, Santana et al. (2021) observed an anticyclonic eddy propagating downstream from North Cape to the typical location of the ECE (using less than a year of data). All of the long-term mean eddies are detectable down to at least 1,500 m and the WE has been observed to be deeper than 2,000 m (Roemmich & Sutton, 1998).

Off the northern tip of NZ the NCE forms by the partial separation of the EAUC from the coast, believed to be due to the curvature in the alongshore flow (Stanton et al., 1997; Stevens et al., 2019). The strength and position of the EAUC is highly variable with most of the current recirculating around the NCE (Fernandez et al., 2018; Stanton et al., 1997). This region exhibits a high level of mesoscale variability, with an alongshore correlation length scale of ∼100 km, and the south-east flowing EAUC is not always present as a contiguous feature. High-frequency variability (<30 days) observed in the EAUC was shown to be coherent with alongshore wind stress and wind stress curl (Santana et al., 2021).



21699291, 2023, 4, Downloaded from https://agupubs.onlinelibrary.wiley.com/doi/10.1029/2022JC018624 by University of New South Wales, Wiley Online Library on [16/10/2023]. See the Terms and Conditions (https://onlinelibrary.wiley.com/terms-and-conditions) on Wiley Online Library for rules of use; OA articles are governed by the applicable Creative Commons License

The EAUC continues down the northeast coast of the North Island and, at East Cape, the coastline turns sharply and some of the EAUC recirculates to the north east and forms the ECE (Roemmich & Sutton, 1998). The remainder of the EAUC continues south along the shelf break and becomes known as the ECC. At the southern end of the North Island, the ECC separates from the coast and heads eastwards, forming the WE (Chiswell, 2005; Fernandez et al., 2018). The ECC transport is reinforced by recirculation in the WE (Chiswell & Roemmich, 1998). This semi-permanent eddy is deeper than the NCE and the ECE, extending below 2,000 m (Roemmich & Sutton, 1998).

The EAUC converges with the subtropical front (STF) and both currents turn eastward in a confluence region determined by local bathymetry (Fernandez et al., 2014; Ganachaud et al., 2014). Along the southeastern tip of the North Island is the northward flowing Wairarapa Coastal Current, carrying relatively cool and fresh water northwards along the coast inshore of the relatively warmer and more saline ECC (Chiswell, 2000). The Wairarapa Coastal Current transport diminishes northwards as the current becomes entrained into the ECC (Chiswell, 2005).

Off the west coast of the northern North Island, limited observations suggest a weak southeastward mean flow offshore of the 1,000 m isobath, named the West Auckland Current, with a northwestward mean flow found inshore of this (Sutton & Bowen, 2011). The offshore flows appear to result from large-scale SSH gradients, while the inshore flows are complex and wind driven. In general, the flows off the west coast of the North Island are shown to be weak with variability dominated by tidal and intra-annual time scales.

### 2.3. The Circumpolar and STFs

To the south, NZ is influenced by the Southern Ocean circulation and its associated fronts. North of the Antarctic Circumpolar Current (ACC) the Southern Ocean is characterized by a series of circumpolar fronts associated with enhanced meridional gradients in temperature and/or salinity and strong flows (Orsi et al., 1995; Sokolov & Rintoul, 2009). Three primary Southern Ocean fronts are the Subantarctic Front (SAF), the Polar Front and the southern ACC front. Furthermore, the waters of the Southern Ocean are separated from the warmer and saltier subtropical waters by the STF. The SAF and the STF interact with topography south of NZ and feed boundary currents along NZ's South Island (Chiswell et al., 2015; Smith et al., 2013; Tilburg et al., 2002).

East of NZ, the pathway of the STF is determined by forcing of upper-ocean currents by topographically constrained abyssal flow (Tilburg et al., 2002). The pathway of the SAF is strongly influenced by a barotropic response to bottom topography with its associated current flowing along the southern edge of a large submarine platform southeast of NZ (the Campbell Plateau; Morris et al., 2001; Stanton & Morris, 2004).

### 2.4. South Island's Boundary Currents

The STF in the southern Tasman Sea, west of NZ, feeds both a northward-flowing current (the Westland Current, WC) and a southward-flowing current (the Fiordland Current, FC) along the west coast of the South Island (Chandler et al., 2019; Figure 1). Around 41°–44°S weak eastward geostrophic transport associated with the STF impinges on the west coast of the South Island and bifurcates into the WC and the FC (Chiswell et al., 2015; Heath, 1982; Ridgway & Dunn, 2003), providing a pathway for the flow of subtropical water out of the Tasman Sea. The WC is believed to be primarily driven by the prevailing southwest winds (Heath, 1982; Stanton, 1976) and has been shown to be influenced by Coastal-Trapped Waves generated by winds at the Cook Strait (Cahill et al., 1991).

The FC flows poleward along the southern portion of the west coast of the South Island and around the southern tip of NZ (Chandler et al., 2019). This poleward-flowing eastern boundary current is driven by a poleward pressure gradient that opposes the prevailing winds (Chandler et al., 2019; Ridgway & Dunn, 2003), similar to the mechanism driving the Leeuwin Current off the west coast of Australia.

The STF follows a convoluted path south of NZ before turning to flow adjacent to the east coast of the South Island (Chandler et al., 2019; Smith et al., 2013). The Southland Current (SC) flows northward along the east coast of the South Island and is associated with the Southland Front, a local manifestation of the STF, which separates a strip of warm, salty Subtropical Water on the continental shelf from cold, fresh subantarctic water (Hopkins et al., 2010; Sutton, 2003). While the FC and the SC are both associated with the STF, the extent to which the FC is connected to the SC remains unclear (Chandler et al., 2019). The SC advects cold water of mostly (90%) subantarctic origin to the region south of Chatham Rise (Chiswell, 1996; Fernandez et al., 2018; Sutton, 2001).



21699291, 2023, 4, Downloaded from https://agupubs.onlinelibrary.wiley.com/doi/10.1029/2022JC018624 by University of New South Wales, Wiley Online Library on [16/10/2023]. See the Terms and Conditions (https://onlinelibrary.wiley.com/terms-and-conditions) on Wiley Online Library for rules of use; OA articles are governed by the applicable Creative Commons License

### 2.5. Central New Zealand and the Cook Strait

Central NZ's shelf seas are strongly influenced by wind and tidal driven circulation and mixing. The Cook Strait connects the Tasman Sea to the west and the Pacific Ocean to the east and is 22 km wide at its narrowest point with a maximum depth of 350 m and a mean depth of 210 m (Stevens et al., 2019). Flows in the Cook Strait are largely dominated by the semidiurnal tide with a much smaller residual flow from west to east (Stevens, 2014; Walters et al., 2010). The mean residual volume flux through Cook Strait was estimated at 0.42 ± 0.08 Sv compared to the $M_2$ tidal volume flux amplitude of 4.68 Sv, and the subtidal volume flux fluctuations are predominantly wind-driven with a standard deviation of 0.62 Sv (Hadfield & Stevens, 2020). The flow to the east of central NZ is complex; the outflow on the eastern side of central NZ is a combination of water masses from the SC passing northward along the east coast of the South Island, the D'Urville Current exiting the Greater Cook Strait and meanders from the ECC (Bowman et al., 1983; Chiswell, 2000; Heath, 1971).

### 2.6. Ocean Heat Content

Ocean heat content has impacts on weather and marine ecosystems, and understanding its variability and the associated drivers is specifically important for the prediction of marine heatwaves. In the southwest Pacific, Bowen et al. (2017) investigate the dynamics responsible for ocean heat transport convergence to elucidate the drivers of Sea Surface Temperature (SST) variability in the region and find that SST around NZ is connected to regional processes over a wide area of the South Pacific. They show that the inter-annual variability of temperature around NZ cannot be explained by the advection of heat by boundary currents, as it has been on the east coast of Australia (Elzahaby et al., 2021; Hill et al., 2008; Z. Li et al., 2020; Oliver & Holbrook, 2014). Indeed the temperature and UOHC are highly correlated on the west and east coasts of NZ despite marked differences in circulation regimes. Instead, they suggest that ocean heat transport convergence may be due to the adjustment of the thermocline around NZ from the arrival of wind-driven barotropic Rossby waves, while upper ocean temperature anomalies are dominated by air-sea heat fluxes in some years. However, Behrens et al. (2019) show that ocean heat content in the Tasman Sea is primarily controlled by the transport in the EAC and the "gating" between the EAC eastern extension and the EAC southern extension. The thermocline varies coherently in the Tasman Sea and off northeast NZ (Bowen et al., 2017).

## 3. Ocean Model

### 3.1. Model Configuration

We use a 28 yr free-running simulation (the Moana Ocean Hindcast) of the NZ region for this analysis (Azevedo Correia de Souza, 2022). The model is a configuration of the Regional Ocean Modeling System (ROMS) version 3.9 and simulates the atmospherically forced eddying ocean circulation and the tides in the NZ oceanic region. ROMS is a free-surface, hydrostatic, primitive equation ocean model solved on a curvilinear grid with a terrain-following vertical coordinate system (Shchepetkin & McWilliams, 2005). The model has a 5 km horizontal resolution and 50 vertical s-layers.

Initial and boundary conditions are from the GLORYS ocean reanalysis, developed by the Copernicus Marine Environment Monitoring Service. Atmospheric forcing fields from the Climate Forecast System Reanalysis (CFSR) provided by National Center for Atmospheric Research (https://climatedataguide.ucar.edu/climate-data/climate-forecast-system-reanalysis-cfsr) are used to compute the surface wind stress and surface net heat and freshwater fluxes using the bulk flux parameterization of Fairall et al. (1996). Tides are included at the open boundaries as a separate spectral forcing (Janekovic & Powell, 2012) with harmonics provided by the TPXO global tidal solution (Egbert & Erofeeva, 2002). The climatological fluxes from 42 rivers around NZ are included. The model simulation spans from 1 January 1993 to 1 January 2021. A description of the experiment and evaluation against observations is provided by Azevedo Correia de Souza et al. (2022).

### 3.2. Model Validation

To compliment the model validation presented in Azevedo Correia de Souza et al. (2022), we present validation of the model's surface representation in terms of the mean and variability of SSH and SST, and the eddy variability. We use the gridded SSH product from Archiving, Validation and Interpretation of Satellite Oceanographic



21699291, 2023, 4, Downloaded from https://agupubs.onlinelibrary.wiley.com/doi/10.1029/2022JC018624 by University of New South Wales, Wiley Online Library on [16/10/2023]. See the Terms and Conditions (https://onlinelibrary.wiley.com/terms-and-conditions) on Wiley Online Library for rules of use; OA articles are governed by the applicable Creative Commons License

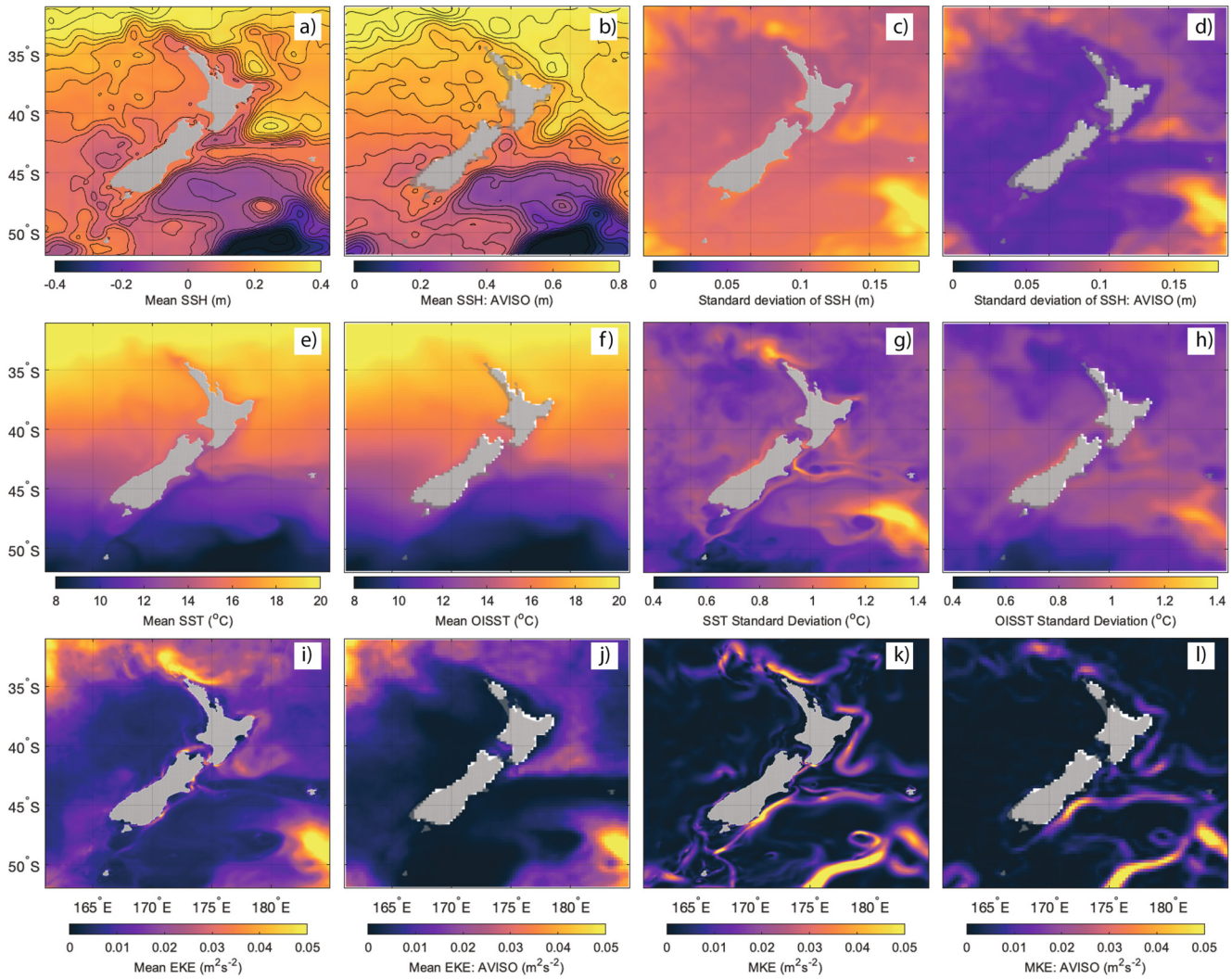


**Figure 2.** Model and observation comparisons for surface fields. Mean Sea Surface Height (SSH) from model (a) and AVISO (b), standard deviation of SSH from model (c), and AVISO (d). Mean SST from model (e) and OISST (f), standard deviation of SST from model (g), and OISST (h) (seasonal cycle removed by harmonic fit). Mean EKE from model (i) and AVISO (j), MKE from model (k), and AVISO (l). Model data is from the daily-average output from the Moana Ocean Hindcast, and observational data is daily.

(AVISO, Ducet et al., 2000) and the gridded SST product from the National Oceanic and Atmospheric Administration Optimum Interpolation (OISST, Huang et al., 2021). Both products are derived from satellite observations and are provided daily with a 0.25° spatial resolution.

The mean modeled SSH field represents well all of the notable features seen in the mean AVISO field (Figures 2a and 2b), including the EAC eastern extension reaching the northern tip of NZ, the NCE, ECE and WE, and the Southland Front off the east coast of the South Island. The modeled mean SSH field shows sharper gradients compared to those implied from satellite observations. Ballarotta et al. (2019) showed that the effective spatial resolution of the altimetry maps around NZ is between 150 and 200 km, marginally resolving the mesoscale eddies, and that the mean temporal resolution of the AVISO altimetry maps ranges between 35 and 42 days around NZ. This means that the mesoscale eddy related variability and the sharp gradients associated with the complex boundary current circulation will be poorly resolved by the AVISO product, and hence it is expected that the model exhibits more variability and higher eddy kinetic energy (EKE; as discussed below). The mean SST is well represented in the model compared to OISST (Figures 2e and 2f). The cooler area directly off North Cape, likely due to tidal mixing and current and mesoscale eddy driven upwelling (Baxter, 2022), is more pronounced in the model compared to the observational product, likely due to the lower resolution of the SST product.



21699291, 2023, 4, Downloaded from https://agupubs.onlinelibrary.wiley.com/doi/10.1029/2022JC018624 by University of New South Wales, Wiley Online Library on [16/10/2023]. See the Terms and Conditions (https://onlinelibrary.wiley.com/terms-and-conditions) on Wiley Online Library for rules of use; OA articles are governed by the applicable Creative Commons License

**Table 1**
*Alongshore Transport (Sv) Through Crossshore Sections (Figure 7, Sections 1–6 and Cook Strait) and the Offshore Sections (Figure 7, Sections A–D)*

| Section | Modeled transport (Sv) | Length (km)/ depth (m) | Other studies transport (Sv) | Data/method |
|---|---|---|---|---|
| 1. EAUC | 10.2 ± 5.71 | 264/750 | 9 (Roemmich & Sutton, 1998) | Altimetry and hydrography, transport to 2,000 m |
| | | | 17 ± 5.3 (including NCE recirculation to 33°*S*), | |
| | | | 9.5 ± 5.5 (excluding recirculation to 31°S) (Stanton & Sutton, 2003) | Current meter arrays 1995–1998, altimetry and CTD data |
| | | | 15–23 (to 33°S), 8–21 (to 31.75°S) (Bowen et al., 2014) | MDT and Argo trajectories |
| | | | 10.5 ± 4.4, 12.4 ± 4.5 (Fernandez et al., 2018) | Altimetry, CTD and XBT data |
| 2. EAUC (*S*th) | 28.0 ± 8.40 | 151/2,300(FD) | 14.8 ± 3.2 (Fernandez et al., 2018) | Altimetry, CTD and XBT data |
| 3. ECC | −37.6 ± 10.2 | 279/3,100(FD) | 10–20 (Chiswell & Roemmich, 1998) > 15 (Chiswell, 2005) | Altimetry and hydrography |
| | | | 10.5 ± 2.7 (*N*th) and 5.6 ± 2.5 (*S*th) (Fernandez et al., 2018) | Altimetry and CTD, relative to 2,000 dbar |
| | | | | Altimetry and hydrography |
| 4.West coast *N*th Island | 3.57 ± 3.65 | 200/1,700(FD) | 0.5 ± 0.7 inshore(30 km) −1.6 ± 1.2 offshore (30–80 km) (Sutton & Bowen, 2011) | Current meter array 2003, <1,200 m depth |
| 5. SC | 9.32 ± 2.66 | 122/1,150(FD) | 10.4 (Chiswell, 1996) | Hydrography |
| | | | 8.3 ± 2.7 (Sutton, 2003) | CTD |
| | | | 7.2 ± 0.8, 10.6 ± 1.0 (Fernandez et al., 2018) | Altimetry and hydrography |
| 6. FC | −4.32 ± 12.4 | 200/3,900(FD) | Velocity structure similar to this study, no transport estimate (Chandler et al., 2019) | Altimetry and MDT |
| 7. WC | 0.0240 ± 1.64 | 200/750(FD) | 0.05 ± 0.3 $ms^{-1}$ (Heath, 1985) | |
| 8. CS | 0.19 ± 0.50 | 15/FD | 0.25 (Stevens, 2014) | Current observations |
| | | | 0.42 ± 0.08 (Hadfield & Stevens, 2020) | Modeling |
| A. North Cape Separation | 14.7 ± 12.3 | 148/3,000(FD) | 9–20 (Roemmich & Sutton, 1998) | Altimetry and hydrography, transport to 2,000 m |
| B. North Cape Separation | 24.7 ± 14.9 | 131/2,050 | 10–15 (Roemmich & Sutton, 1998) | Altimetry and hydrography, transport to 2,000 m |
| C. Wairarapa Separation | 42.0 ± 11.1 | 150/2,700(FD) | 15 (Chiswell, 2005) | Altimetry and CTD, relative to 2,000 dbar |
| D. Wairarapa Separation | 10.8 ± 4.79 | 149/990(FD) | | |

*Note.* FD, Full Depth, MDT, Mean dynamic topography.

The surface geostrophic velocities computed from the 0.25° AVISO SSH mapped product are used to compute EKE and mean kinetic energy (MKE). MKE is given by $MKE = \frac{1}{2}\left(\bar{U}^2 + \bar{V}^2\right)$, where $\bar{U}$ and $\bar{V}$ are the time mean velocity components, and the EKE is given by $EKE = \frac{1}{2}\left(U'^2 + V'^2\right)$, where $U'$ and $V'$ are the velocity anomalies. The MKE describes the energy associated with the mean currents, while the EKE describes the energy associated with the perturbations from the mean. The match between modeled and observed MKE is fairly good for the coherent boundary current regions, but the model has higher MKE across the EAUC and ECC. As discussed above and in Azevedo Correia de Souza et al. (2022), gradients in SSH are generally stronger in the model, specially in the EAUC and ECC regions, resulting in sharper fronts and stronger boundary currents, compared to those implied from satellite observations. If the fine scale SSH variability is not resolved by the AVISO fields (Ballarotta et al., 2019), then the geostrophic velocities will be underestimated even in the mean. Indeed the MKE inferred from AVISO is considerably lower in the EAUC compared to the more coherent SC (Figure 2l), despite both currents having similar volume transports (refer to Section 4.2 and Table 1), while the modeled MKEs are similar (Figure 2k).

High-modeled SSH variability occurs off North Cape and in the WE region, with SSH variability the lowest off the west coast of the North Island and over the Campbell Plateau and Chatham Rise (Figures 2c and 2d). The SSH (Figures 2c and 2d) and SST (Figures 2g and 2h) variability are greater in the model (5 km resolution) than in AVISO and OISST, respectively, but show similar spatial structure with the exception of the region off North



21699291, 2023, 4, Downloaded from https://agupubs.onlinelibrary.wiley.com/doi/10.1029/2022JC018624 by University of New South Wales, Wiley Online Library on [16/10/2023]. See the Terms and Conditions (https://onlinelibrary.wiley.com/terms-and-conditions) on Wiley Online Library for rules of use; OA articles are governed by the applicable Creative Commons License

Cape. This variability is associated with the interaction of the EAUC and North Cape (the NCE) with variability at temporal and spatial scales not well resolved by the satellite observations (discussed above). While the model shows larger overall SSH and SST variance, Azevedo Correia de Souza et al. (2022) show that the longer time scale (seasonal to inter-annual) variability of the SSH throughout the domain is well reproduced.

Modeled EKE is higher than that inferred from the AVISO product geostrophic velocities, as mesoscale eddy related variability is poorly resolved by the AVISO product. The spatial structure of mean EKE is well represented by the model, again with the exception of the EKE off North Cape where variability is dominated by spatial scales not well resolved by altimetry. Furthermore, the model will contain contribution from ageostrophic processes. Stanton and Sutton (2003) report EKE values as high as 0.031 $m^2s^{-2}$ off North Cape from along-track altimetry, higher than the mean EKE from AVISO reported here (Figure 2j). This analysis suggests that NZ's complex system of boundary currents is associated with sharp gradients and variability on temporal and spatial scales that are poorly resolved by satellite observations.

In general, the model represents NZ's major boundary currents well (Figure 1). In Section 4 and Table 1 of this paper, we present a detailed comparison of the boundary current transport estimated from the model with existing studies in the literature. We reinforce the validity of the subsurface structure of the model by the comparisons of the three-dimensional structure of the boundary currents with various modeling and observational studies.

## 4. Boundary Currents

### 4.1. Eddy Variability

The modeled SSH and surface velocity fields are analyzed to elucidate the mean surface circulation and eddy variability across the region. MKE (Figure 2k) clearly shows NZ's defined boundary currents; the strongest being the EAUC and its continuation into the ECC, and the SC. The regions of highest model SSH variability (Figure 2c) and EKE (Figure 2i) are off North Cape and in the regions associated with the shedding of the ECE and the WE. The ratio of MKE to the mean EKE (not shown) describes the degree of coherence of an ocean current. The EAUC has the highest eddy variability off North Cape; as it evolves downstream and becomes the ECC eddy variability is lower and the current is more coherent. The SC and the EAUC have similar MKE, but the SC is much more coherent (larger ratio of MKE to mean EKE). Mean EKE is the lowest of the region off the west coast of NZ and over the Campbell Plateau.

There is a notable division in EKE between the north and south off the east coast of NZ (Figure 2i) where the topography of the Chatham Rise (Figure 1a) divides the two flow regimes by constraining the latitudinal movement of the STF (Chiswell, 2001). The model displays a sharp SSH gradient along the north of the Chatham Rise (Figure 2a) and a narrow westward flowing counter-current directly north of the rise (centered on 43°S, Figure 1c), consistent with observations by Chiswell (2001). This narrow current and sharp SSH ridge could not be well resolved by AVISO, and their existence warrants further investigation. While Chiswell (2000) suggest the WCC has origins from the D'Urville Current (from the Cook Strait) and the SC, the model results suggest the current may also have origins from over the Chatham Rise (refer forward to Figure 7).

EKE displays distinct seasonality (Figure 3) particularly in the regions influenced by the EAC eastern extension, the EAUC and the ECC. Across the EAUC and ECC system, EKE is greatest in Austral summer and reduces in the downstream direction through autumn to reach a minimum throughout in winter. Again from August to December (spring-summer) the EKE increases gradually in the downstream direction.

### 4.2. Transport and Mean Structure

The modeled mean surface currents (Figure 1c) and depth-integrated currents (Figure 7) show NZ's major boundary currents. Here, we investigate current depth structure, transport, and variability. The high-resolution, 3-dimensional, long-duration hindcast of the entire NZ region allows the boundary currents to be characterized using a seamless approach across the region. We choose seven shore-normal sections to pass through NZ's major boundary currents where the flow is maximum (Figure 1c, Sections 1–6) and four sections where major boundary currents turn offshore (Figure 1c, sections A–D). We also report modeled transport through the Cook Strait. The subsurface velocity structure through the sections is shown for the North Island boundary currents (Figure 4), the South Island boundary currents (Figure 5), and the offshore currents (Figure 6).



21699291, 2023, 4, Downloaded from https://agupubs.onlinelibrary.wiley.com/doi/10.1029/2022JC018624 by University of New South Wales, Wiley Online Library on [16/10/2023]. See the Terms and Conditions (https://onlinelibrary.wiley.com/terms-and-conditions) on Wiley Online Library for rules of use; OA articles are governed by the applicable Creative Commons License

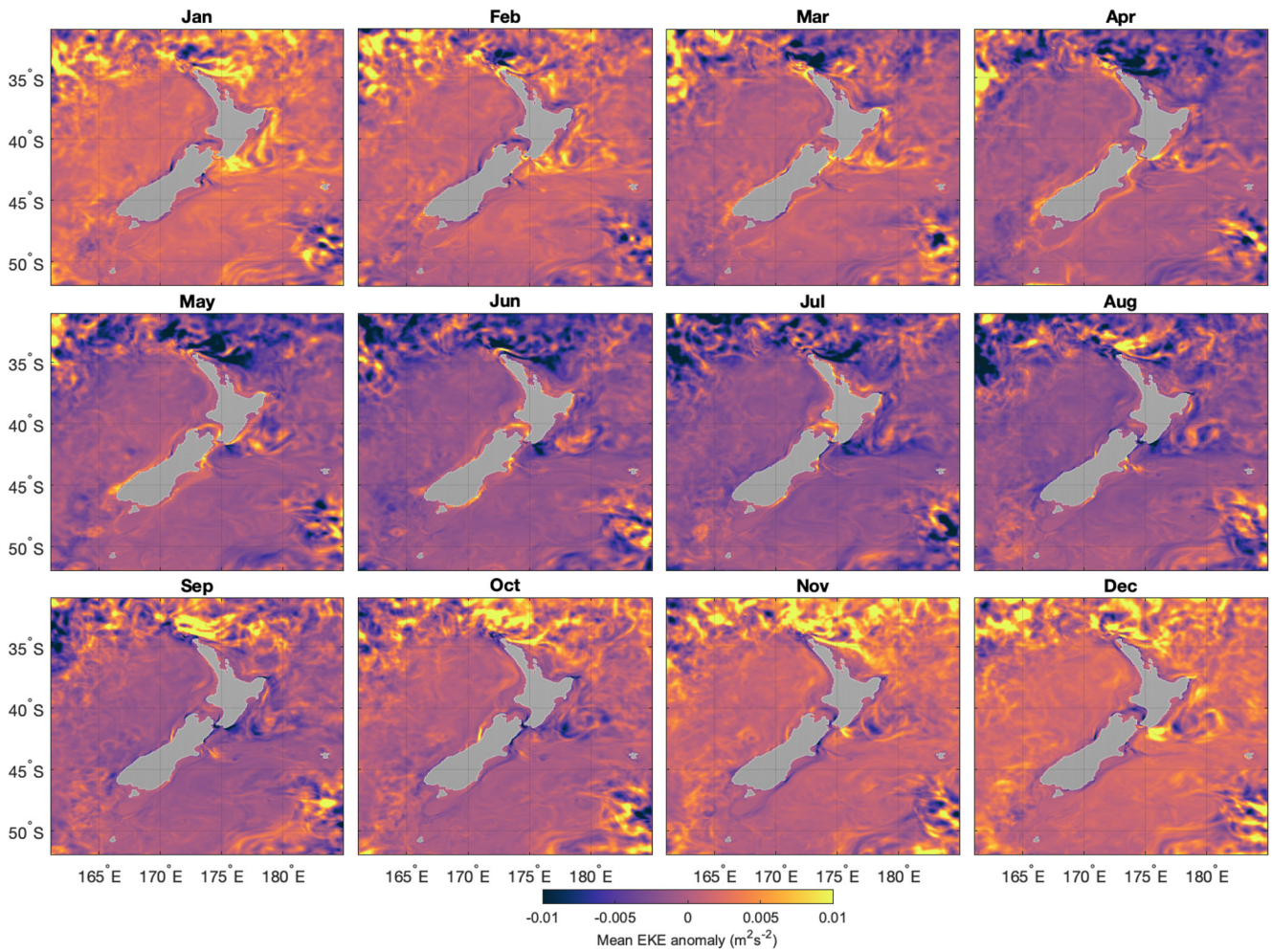


**Figure 3.** Surface Eddy Kinetic Energy (EKE) anomalies with month showing EKE seasonality.

The volume transport in Sverdrups (Sv) through each section is computed daily and is given by,

$$Trans = \frac{1}{10^6} \int_{-D}^{0} \int_{x_0}^{x_i} (\mathbf{v}) dx dz, \tag{1}$$

where $x_0$ to $x_i$ is the cross-shore distance and -D is the depth of the section, **v** is the daily-averaged across-section velocity. The mean and standard deviation of the daily-averaged current transport are shown in Figures 4–6. We choose the cross-sectional area over which to compute current transport based on the mean alongshore velocity sections. The section length and depth over which the transport is computed is defined by the $\pm 0.05$ ms$^{-1}$ contour (the sign depending on the mean flow direction) in the velocity mean (as per Kerry & Roughan, 2020), except in cases where there is no defined core in which case a distance of 200 km offshore is chosen (i.e., Fiordland Current, Westland Current and west coast of NZ). Table 1 summarizes the current transports (adapted from Azevedo Correia de Souza et al., 2022) and presents comparisons to previous estimates. The differences are discussed below.

#### 4.2.1. North Island

The mean EAUC extends 264 km offshore with two distinct cores centered on about 55 and 200 km offshore (Figure 4a). The depth of the mean EAUC core is 750 m (to the +0.05 ms$^{-1}$ velocity contour), consistent with observations presented in Santana et al. (2021). The modeled mean alongshore transport across the section is 10.2 ± 5.71 Sv to the southeast, consistent with the estimate of 9 Sv from mean hydrographic climatology by Roemmich and Sutton (1998), 9.5 ± 5.5 Sv from altimetry and CTD data by Stanton and Sutton (2003), 8–15 Sv



21699291, 2023, 4, Downloaded from https://agupubs.onlinelibrary.wiley.com/doi/10.1029/2022JC018624 by University of New South Wales, Wiley Online Library on [16/10/2023]. See the Terms and Conditions (https://onlinelibrary.wiley.com/terms-and-conditions) on Wiley Online Library for rules of use; OA articles are governed by the applicable Creative Commons License

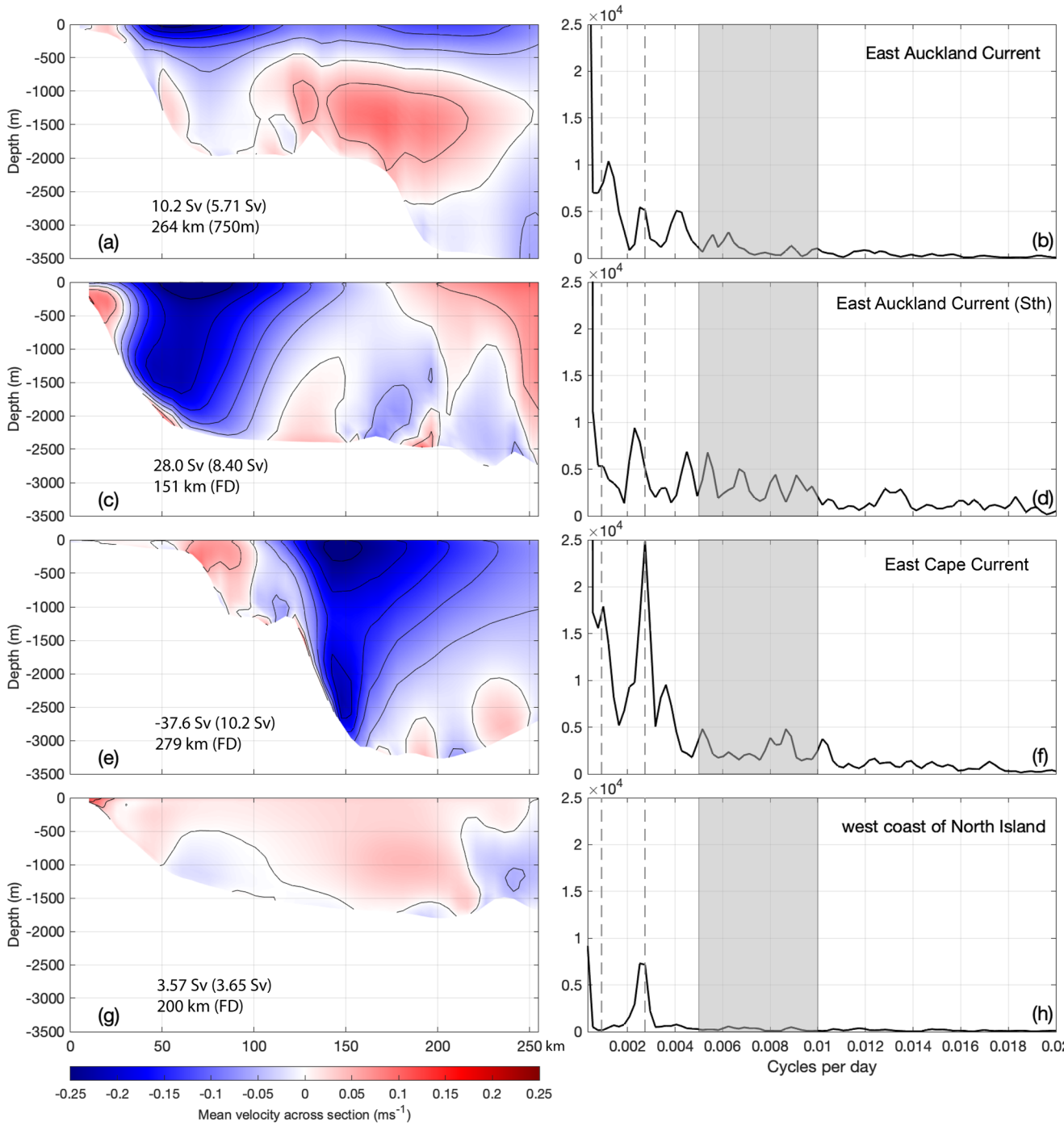


**Figure 4.** Shore normal sections through the North Island boundary currents. Mean alongshore velocity with mean velocity contours every 0.05 ms$^{-1}$ (a, c, e, g). Note that the main core of the East Auckland Current (EAUC) and the EAUC (South) flow to the east-southeast which is defined as negative in the figure, to be consistent with the negative southward flowing East Cape Current. Mean alongshore transport (and standard deviation of alongshore transport) and the section length (and depth) over which the transport is computed are shown. FD, Full Depth. Frequency spectra of daily averaged volume transport (b, d, f, h). On the frequency spectra the gray shaded area shows periods of 100–200 days and the gray dashed lines show the frequencies associated with (from left to right) 3-yearly periods and the annual period.

derived from Argo float trajectories in the same region (Bowen et al., 2014), and 8.4–12.5 Sv from long-term data from altimetry, XBT measurements, and CTD casts (Fernandez et al., 2018; Table 1). EAUC transport is of comparable magnitude to the total mean transport exiting the EAC system to the east, which is estimated to be 8–12 Sv and with the current extending to about 500–800 m (Kerry & Roughan, 2020; Sutton & Bowen, 2014;



21699291, 2023, 4, Downloaded from https://agupubs.onlinelibrary.wiley.com/doi/10.1029/2022JC018624 by University of New South Wales, Wiley Online Library on [16/10/2023]. See the Terms and Conditions (https://onlinelibrary.wiley.com/terms-and-conditions) on Wiley Online Library for rules of use; OA articles are governed by the applicable Creative Commons License

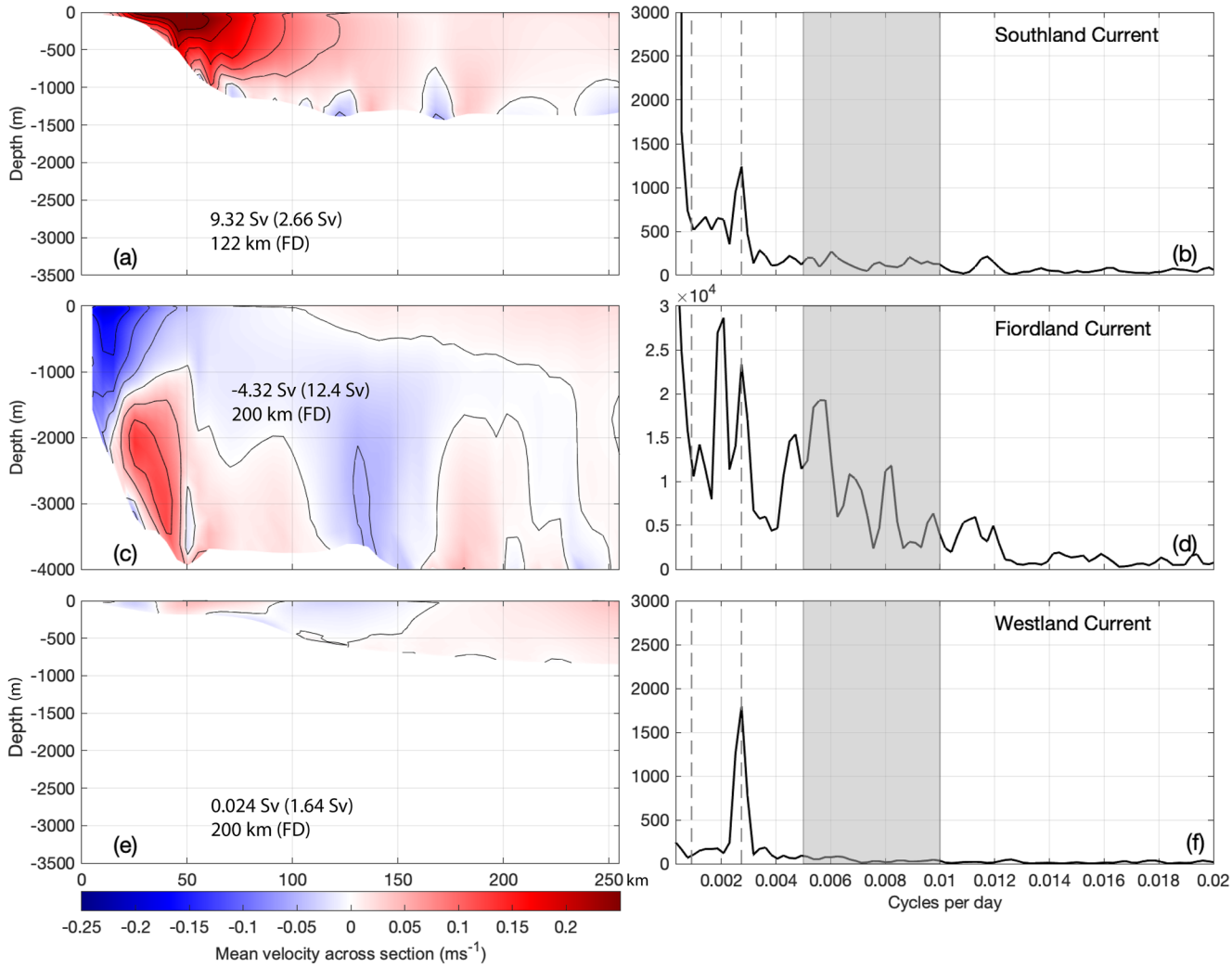


**Figure 5.** Shore normal sections through the South Island boundary currents. Mean alongshore velocity with mean velocity contours every 0.05 ms$^{-1}$ (a, c, e). Mean alongshore transport (and standard deviation of alongshore transport) and the section length (and depth) over which the transport is computed are shown. FD, Full Depth. Frequency spectra of daily averaged volume transport (b, d, f). On the frequency spectra the gray shaded area shows periods of 100–200 days and the gray dashed lines show the frequencies associated with (from left to right) 3-yearly periods and the annual period.

Ypma et al., 2016). In the EAUC, the opposing flow at depth on the shelf slope (Figure 4a) was also observed by Santana et al. (2021) and Stanton and Sutton.

Recirculation in the NCE feeds back into the EAUC and results in a deepening of the current (Figure 7). Likewise, recirculation in the ECE and the WE causes further deepening and strengthening of the current (Figures 4a, 4c, 4e, and 7). This is consistent with the results of Roemmich and Sutton (1998) who show that the WE is deeper than the NCE and the ECE, extending below 2,000 m. This downstream strengthening and deepening also occurs in the EAC (Kerry & Roughan, 2020), and in the Kuroshio (Andres et al., 2017).

The modeled mean transport in the EAUC increases from 10.2 Sv (Section 1, Figure 1c) to 28 Sv as it flows eastwards north of East Cape (Section 2) and is strengthened by recirculation in the ECE. Mean modeled transport further increases to 37.6 Sv south of East Cape (Section 3) where it is strengthened by recirculation in the WE. Our estimates of ECC transport are considerably greater than estimates presented to date in the literature of 10–20 Sv (Chiswell & Roemmich, 1998), 15 Sv (Chiswell, 2005) and 5.6–10.5 Sv (Fernandez et al., 2018), however key differences in the calculation methods and locations exist.

Specifically, these attempts to estimate transport use satellite altimetry combined with subsurface observations to estimate the vertical structure of the current, and assume a level of no motion of 2,000 dbar. As discussed in



21699291, 2023, 4, Downloaded from https://agupubs.onlinelibrary.wiley.com/doi/10.1029/2022JC018624 by University of New South Wales, Wiley Online Library on [16/10/2023]. See the Terms and Conditions (https://onlinelibrary.wiley.com/terms-and-conditions) on Wiley Online Library for rules of use; OA articles are governed by the applicable Creative Commons License

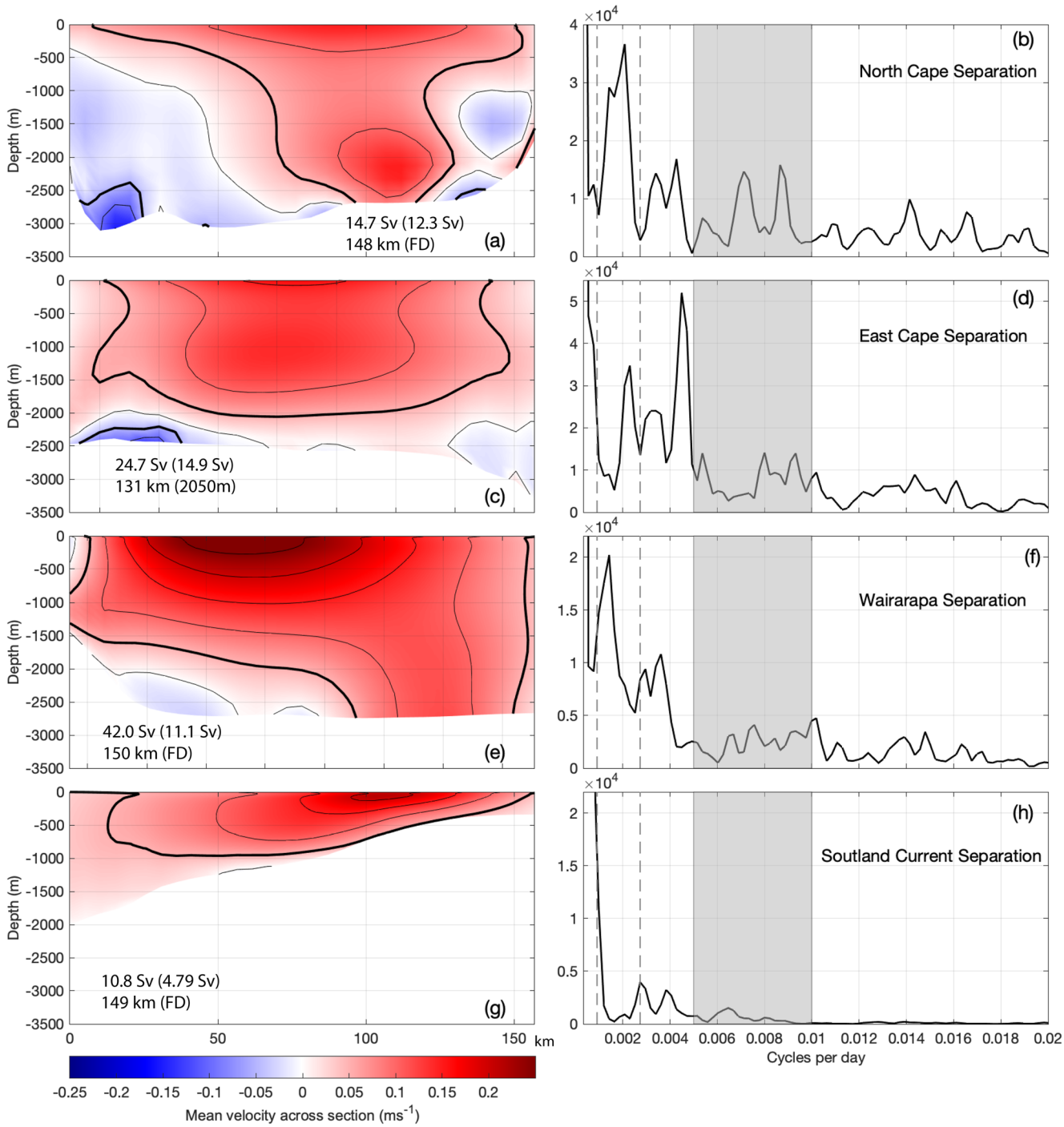


**Figure 6.** Offshore sections. Mean cross-section velocity with mean velocity contours every 0.05 ms$^{-1}$ (a, c, e, g). Mean cross-section transport (and standard deviation of transport) and the section length (and depth) over which the transport is computed are shown. FD, Full Depth. Frequency spectra of daily averaged volume transport (b, d, f, h). On the frequency spectra the gray shaded area shows periods of 100–200 days and the gray dashed lines show the frequencies associated with (from left to right) 3-yearly periods and the annual period.

Section 3.2, the sharp gradients associated with the boundary current circulation are poorly resolved by satellite altimetry products. Furthermore, we show that the ECC extends below 2,000 m, consistent with other studies that have found substantial velocities below 2,000 m in the EAUC and ECC regions (Chiswell, 2003; Roemmich & Sutton, 1998; Sutton & Chereskin, 2002). We find a mean transport of 5 Sv below 2,000 m, with 32.6 Sv above 2,000 m, so the flow below 2,000 m cannot itself explain our considerably greater estimates. Moreover, previous



21699291, 2023, 4, Downloaded from https://agupubs.onlinelibrary.wiley.com/doi/10.1029/2022JC018624 by University of New South Wales, Wiley Online Library on [16/10/2023]. See the Terms and Conditions (https://onlinelibrary.wiley.com/terms-and-conditions) on Wiley Online Library for rules of use; OA articles are governed by the applicable Creative Commons License

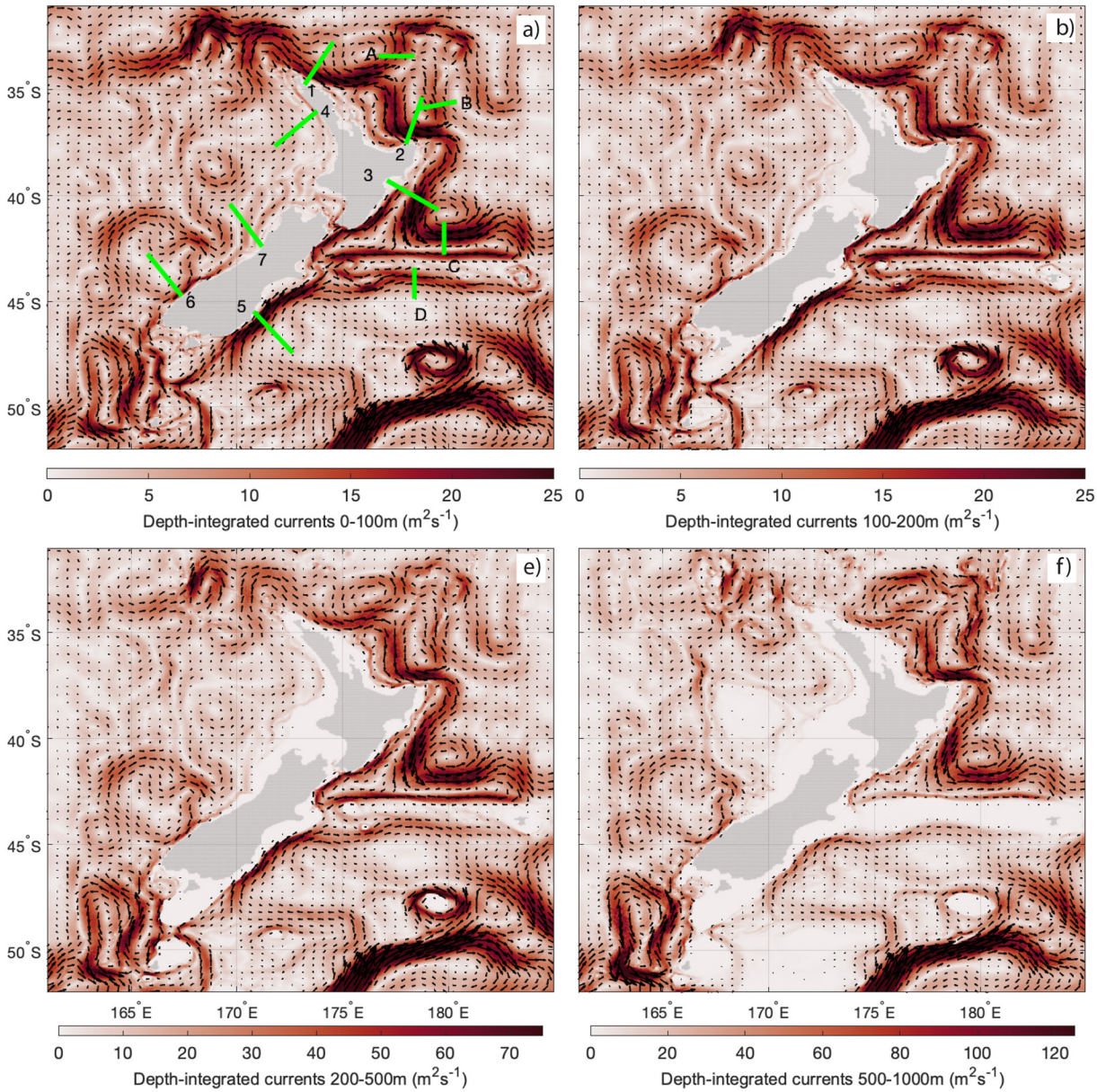


**Figure 7.** Mean depth-integrated current speed and velocity vectors for 0–100 m (a), 100–200 m (b), 200–500 m (c), and 500–1,000 m (d). Data is from the daily-average output from the Moana Ocean Hindcast. Sections for velocity cross-sections and transport calculations are shown as in Figure 1. Note that the color bars are adjusted to account for the depth ranges such that the plots are directly comparable.

estimates have attempted to separate the recirculation driven by the semi-permanent eddies, while our estimates include this recirculation. As shown by Stanton and Sutton (2003), transport estimates are highly sensitive to the distance offshore over which transport is calculated.

The ECC transects of Fernandez et al. (2018) are to the north and to the south of our chosen transect and they estimate mean and standard deviation of volume transports of 10.5 Sv (2.7 Sv) and 5.6 Sv (2.2 Sv), respectively. The transect that is further to the north (directly off East Cape) is located where current velocities are considerably lower and upstream of the influence of the recirculating WE (Figures 1c and 7). The transect to the south is downstream of the peak current velocity and does not capture the recirculating WE (Figure 7). Notably, Fernandez et al. (2018) separate the core transport of the current from the recirculation driven by the "semi-permanent" WE by computing over time-variant sections, while we choose to include this eddy driven transport and compute transport through a time-invariant section. They also note that calculations given a time-invariant offshore point result in differences in transport magnitude, particularly in the ECC.



21699291, 2023, 4, Downloaded from https://agupubs.onlinelibrary.wiley.com/doi/10.1029/2022JC018624 by University of New South Wales, Wiley Online Library on [16/10/2023]. See the Terms and Conditions (https://onlinelibrary.wiley.com/terms-and-conditions) on Wiley Online Library for rules of use; OA articles are governed by the applicable Creative Commons License

Our transport estimate encompasses the entire cross-section through the ECC (based on the 0.05 m $s^{-1}$ mean velocity contour) extending 279 km offshore and to the full water depth (below 3,000 m). Our section was chosen where the ECC shows the strongest velocities, and transport is considerably strengthened due to recirculation of the WE. Roemmich and Sutton (1998) estimated the mean transport in the EAUC system to be 9 Sv with an additional 10 Sv or more of circulation in the eddies, noting that the mean field around northeastern NZ has considerable mesoscale structure. Chiswell and Roemmich (1998) estimate the ECC transport to be 10–20 Sv and Chiswell (2005) estimate the transport in the ECC feeding the WE to be 15 Sv relative to the 2,000 dbar, yet they note that this is likely to be an underestimate as the current core extends deeper than the 2,000 dbar (Chiswell, 2003).

Separation in the EAUC occurs at three distinct locations corresponding to the existence of the three semi-permanent eddies: the NCE, the ECE, and the WE (Sections A, B, and C respectively, Figures 1c and 1). The modeled mean transport in these eddies is 14.7 Sv, 24.7 and 42.0 Sv, respectively, consistent with the downstream strengthening of the current system. The eddy transports are higher than previously reported results, particularly the ECC and WE, as discussed above.

Our study is the first study that we are aware of that has estimated transport in the ECC to include transport due to recirculation in the eddies and that suggests a downstream deepening and strengthening of the EAUC and ECC system. We note that the model provides very consistent estimates of the upstream EAUC mean and variability in transport, as well as the current's 3-dimensional structure, off North Cape (Section 1), as discussed above. The model estimates suggest flow in the ECC is of comparable magnitude to that in the EAC (Kerry & Roughan, 2020), yet the surface MKE plots inferred from the AVISO product show considerably weaker flow in the ECC compared to the EAC (Figure 1a). Both the MKE and mean EKE are lower in the ECC (Figure 2) compared to the EAC (Figure 1 of J. Li et al., 2021). However, the EAC has been estimated to have a maximum core depth of 1,200 m with a core width of 150–200 km (Kerry & Roughan, 2020), while substantial velocities have been found below 2,000 m in the EAUC and ECC regions (Chiswell, 2003; Roemmich & Sutton, 1998; Sutton & Chereskin, 2002), and our transport sections extend to 2,500–3,000 m depth for the EAUC (*S*th) and ECC sections. As such, the ECC may have comparable transport to the EAC despite lower surface MKE and EKE values. Furthermore, the sharp gradients associated with the ECC may be poorly resolved by altimetry (refer to the differences between Figures 2a and 2b). There is no net drift in transport estimates over the hindcast period. Our model estimates of the ECC transport require further validation, which could be achieved with targeted observations, specifically the significant downstream deepening and strengthening in the model. If confirmed, the results may suggest a significant new understanding of this WBC system.

On the west coast of the North Island, a large-scale residual equatorward flow exists with a surface intensified coastal current (Figure 4g). In the coastal jet the mean flow is of the same order as the standard deviation, and outside of the jet the standard deviation exceeds the mean. This is somewhat consistent with the results of Sutton and Bowen (2011) who, using a 1 yr current meter array, show a weak southeastward mean flow offshore of the 1,000 m isobath, with a northwestward mean flow found inshore of this.

#### 4.2.2. South Island

At the west coast of the South Island, bifurcation of the eastward geostrophic transport associated with the STF (3 Sv, Stevens et al., 2019; Stramma et al., 1995) into the FC and the WC occurs where there is an abrupt change in topography (Figure 1b). The FC flows poleward adjacent to the steep shelf break and the WC flows equatorward along the shallow shelf (Figures 5c and 5e). Both the FC and the WC transport have high variability compared to their means. The mean poleward transport from the hindcast in the FC is 4.3 Sv (standard deviation 12.4 Sv), with the WC being much weaker (0.024 Sv, with standard deviation of 1.64 Sv; Table 1). The poleward FC core is centered about 15 km offshore with surface poleward flow extending to 95 km offshore, and a deep (below 1,000 m) equatorward countercurrent offshore of the 2,000 m isobath. The results are consistent with Chandler et al. (2019) who show, from observations, the existence of a stronger inner current about 17.4 km offshore, and a weaker outer current extending to 73.1 km offshore. The weak, equatorward mean flow in the WC of about 0.05 $ms^{-1}$ is consistent with results of Heath (1982); Heath (1985) and is driven by prevailing southeast winds.

The mean structure of the SC (Figure 5a) is consistent with observations in Sutton (2003), and the mean and standard deviation of transport from the hindcast (9.3 and 2.7 Sv) match very well with the mean and standard deviation of their eight observational studies (mean of 8.3 Sv and standard deviation of 2.7 Sv). Similar values



21699291, 2023, 4, Downloaded from https://agupubs.onlinelibrary.wiley.com/doi/10.1029/2022JC018624 by University of New South Wales, Wiley Online Library on [16/10/2023]. See the Terms and Conditions (https://onlinelibrary.wiley.com/terms-and-conditions) on Wiley Online Library for rules of use; OA articles are governed by the applicable Creative Commons License

(10.4 Sv) have been reported by Chiswell (1996), inferred from geostrophic velocities estimated from a 1 yr long CTD survey. More recently, Fernandez et al. (2018) derived the SC volume transport from 1993 to 2012 altimeter data across two sections, south and north of our reference section, reporting 7.2 ± 0.8 Sv and 10.6 ± 1.0 Sv, respectively. In contrast to the EAUC/ECC system, the depth of the SC is constrained by topography and does not change over the alongshore extent of the current (Figure 7). Outflow along the southern ridge of the Chatham Rise (Section D, Figures 1c and 1, Figure 6g) has a mean transport of 10.8 Sv, approximately balancing the SC transport.

#### 4.2.3. Cook Strait

While flows in the Cook Strait are largely tidally dominated, the residual sub-tidal flow is significant as it dominates the net transport of heat and materials (Stevens, 2014). The Cook Strait section in our model is ≈ 15 km wide (represented by only three grid cells), compared to, in reality, a 22 km wide strait at its narrowest region. The mean modeled transport across the Strait is 0.19 ± 0.50 Sv. The high standard deviation relative to the mean illustrates the variable nature of the residual transport. Stevens (2014) estimated a mean transport of 0.25 Sv based on residual (low-passed filtered at 48 hr) currents from 20-month continuous ADCP measurements and Hadfield and Stevens (2020) estimate a 3 yr mean volume flux of 0.42 Sv ± 0.08 Sv based on modeled-measured adjustments. While our model resolution only permitted the Cook Strait to be represented by three grid cells at its narrowest point, we feel it necessary and useful to acknowledge the Cook Strait and to report the modeled transport. It can be expected that the mean transport is sensitive to the time period over which the mean is taken and that the variability is sensitive to the sampling frequency. Our reported values are computed from daily transport estimates over the 28 yr model simulation, so provide a considerably longer time-series than previous estimates (for a potentially more reliable mean estimate) and a higher sampling frequency (for a potentially more reliable estimate of variability). High-resolution modeling combined with a long-term observational campaign would be required to further understand the details of Cook Strait flows.

### 4.3. Variability

Frequency spectra of across-section transport are shown adjacent to the mean sections in Figures 4–6. Variability in modeled EAUC transport is dominated by periods longer than 100 days (Figure 4b), consistent with Santana et al. (2021) and Stanton and Sutton (2003). The EAUC (*S*th) has more energy in the 100–200 days range (Figure 4d), associated with mesoscale eddy variability, while the ECC (Figure 4f) has similar energy in the 100–200 days range, and an annual peak that is much stronger than at the upstream sections. This is similar to the EAC system where a strong annual peak is seen in transport off Sydney (34°S), associated with the seasonality in EKE where recirculating eddies strengthen the transport at this latitude (Kerry & Roughan, 2020). The EAUC, the EAUC (*S*th) and the ECC are all stronger during the summer (Figure 8), however significant seasonal differences in volume transport (outside of the monthly standard deviations) exist only in the ECC.

Fernandez et al. (2018) estimate ECC transport, using altimetry and in situ observations, and purposely exclude eddy driven transport. Our ECC transport estimates include eddy driven transport and are quite different to those of Fernandez et al. (2018) as the two studies are not estimating the same quantity. The differences may also stem from potential shortcomings in the model. However, the seasonality is consistent across both studies with weaker flow in winter and stronger flow in summer. We show an increase in seasonality in current transport as the EAUC/ECC system evolves downstream (Figures 4b, 4d, and 4f), with the strongest transport in the ECC in summer (Figure 8c) associated with higher EKE in the region in summer (Figure 3). Consistent with findings in the EAC (Kerry & Roughan, 2020), this may suggest an increase in eddy driven transport in summer and as the current evolves downstream.

On the west coast of the North Island transport variability at the annual scale dominates (Figure 4h) with significantly stronger flow in early summer and weakest flow in autumn (Figure 8), likely due to seasonality in the prevailing winds (Sutton & Bowen, 2011).

The SC shows a strong annual signal in transport with little energy at shorter periods (Figure 5b), consistent with the highly coherent nature of the SC. SC transport is strongest in Autumn to Winter (Figure 8) and weakest in late Spring to early Summer, consistent with results of Fernandez et al. (2018) and with the finding that Southland Front gradients are strongest during the winter (Chiswell, 1996; Hopkins et al., 2010; Sutton, 2003).

The FC shows high variability at periods around 200 days, a strong annual peak, and a peak at periods greater than a year (Figure 4d). Variability over various temporal scales occurs in the FC, which is driven by both an



21699291, 2023, 4, Downloaded from https://agupubs.onlinelibrary.wiley.com/doi/10.1029/2022JC018624 by University of New South Wales, Wiley Online Library on [16/10/2023]. See the Terms and Conditions (https://onlinelibrary.wiley.com/terms-and-conditions) on Wiley Online Library for rules of use; OA articles are governed by the applicable Creative Commons License

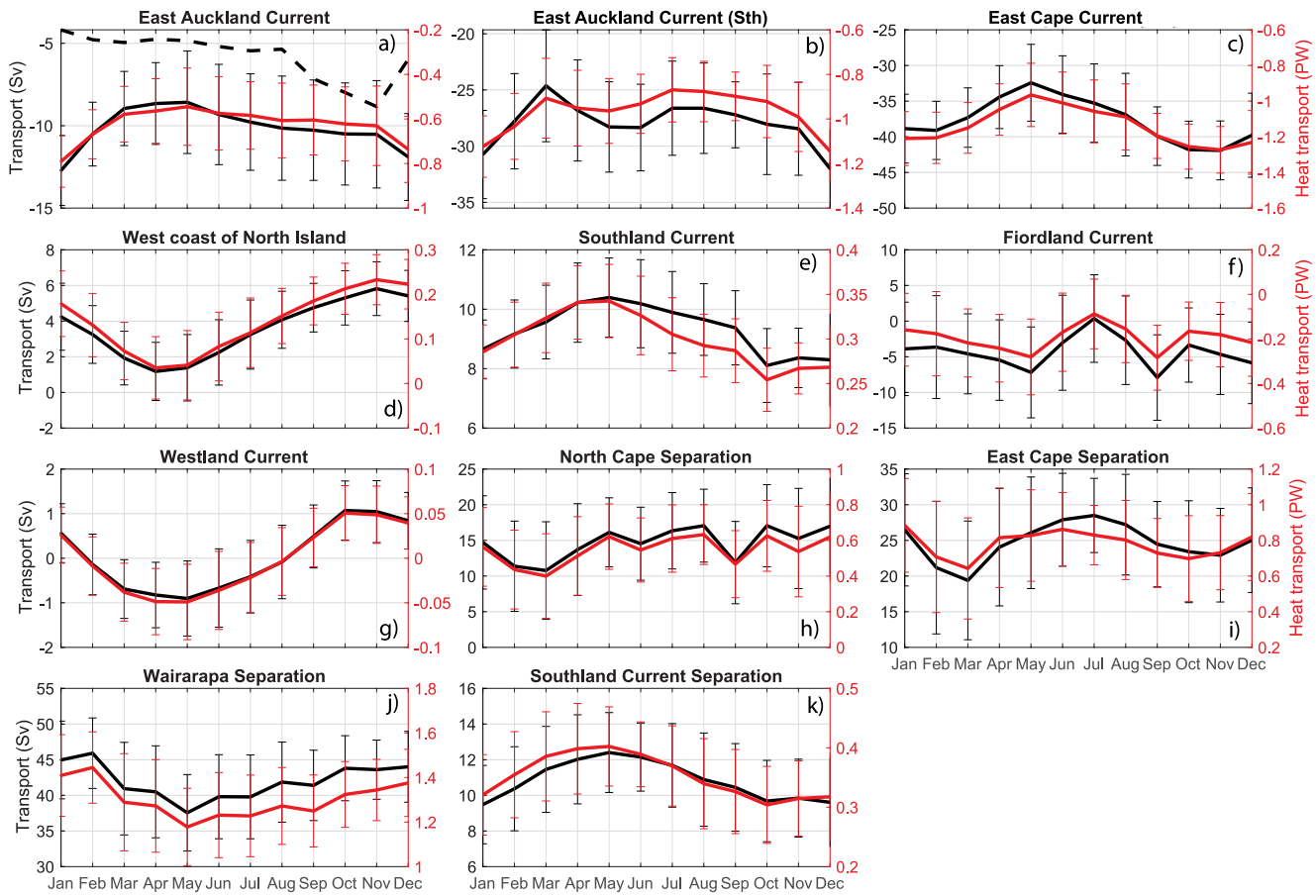


**Figure 8.** Monthly volume and heat transport through the current sections. For the East Auckland Current (EAUC), solid lines are for the current to 264 km offshore, while the dashed line represents volume transport within the coastal jet to 147 km offshore (refer to Figure 4a).

alongshore pressure gradient and wind stress, which often opposes the dominate poleward pressure gradient forcing (Chandler et al., 2019). The WC has a strong annual peak with very little energy at other periods (Figure 4f), due to seasonality in the driving southwest winds (Heath, 1982; Stevens et al., 2019), and seasonal differences in volume transport are significant (Figure 8).

Transport in the three semi-permanent eddies associated with the EAUC/ECC system (Sections A, B, and C respectively, Figure 7, corresponding to the NCE, the ECE, and the WE) has strong variability at periods greater than 200 days with no distinct annual peak (Figures 6b, 6d, and 6f). The ECC separation transport displays a strong peak at 220 days. In contrast, the SC separation shows a strong annual peak (Figure 6h), consistent with the strong seasonality in the SC, and a peak at 260 days.

## 5. Ocean Heat Content

### 5.1. SST

We begin by characterizing SST as this is the most commonly studied metric relating to ocean heat content due to the availability of satellite observations. In the model, high SST variability (Figure 2g) occurs off North Cape, in the regions where the ECE and WEs are shed, and in the confluence region of the Southland Front with the ECC (studied by Greig & Gilmour, 1992; Shaw & Vennell, 2000), as well as along the west coast of the South Island. Seasonal variability in SST is highest in coastal regions of the North Island, the east coast of the South Island and the oceanic region influenced by the confluence of the STF and the SAF (Figure 9a). Seasonality in SST is notably less pronounced off North and East Capes, in the Cook Strait and in the SC. The phase of the seasonal cycle in SST is coherent over most of the domain, except in the regions influenced by the SAF (Figure 9b) suggesting different drivers.



21699291, 2023, 4, Downloaded from https://agupubs.onlinelibrary.wiley.com/doi/10.1029/2022JC018624 by University of New South Wales, Wiley Online Library on [16/10/2023]. See the Terms and Conditions (https://onlinelibrary.wiley.com/terms-and-conditions) on Wiley Online Library for rules of use; OA articles are governed by the applicable Creative Commons License

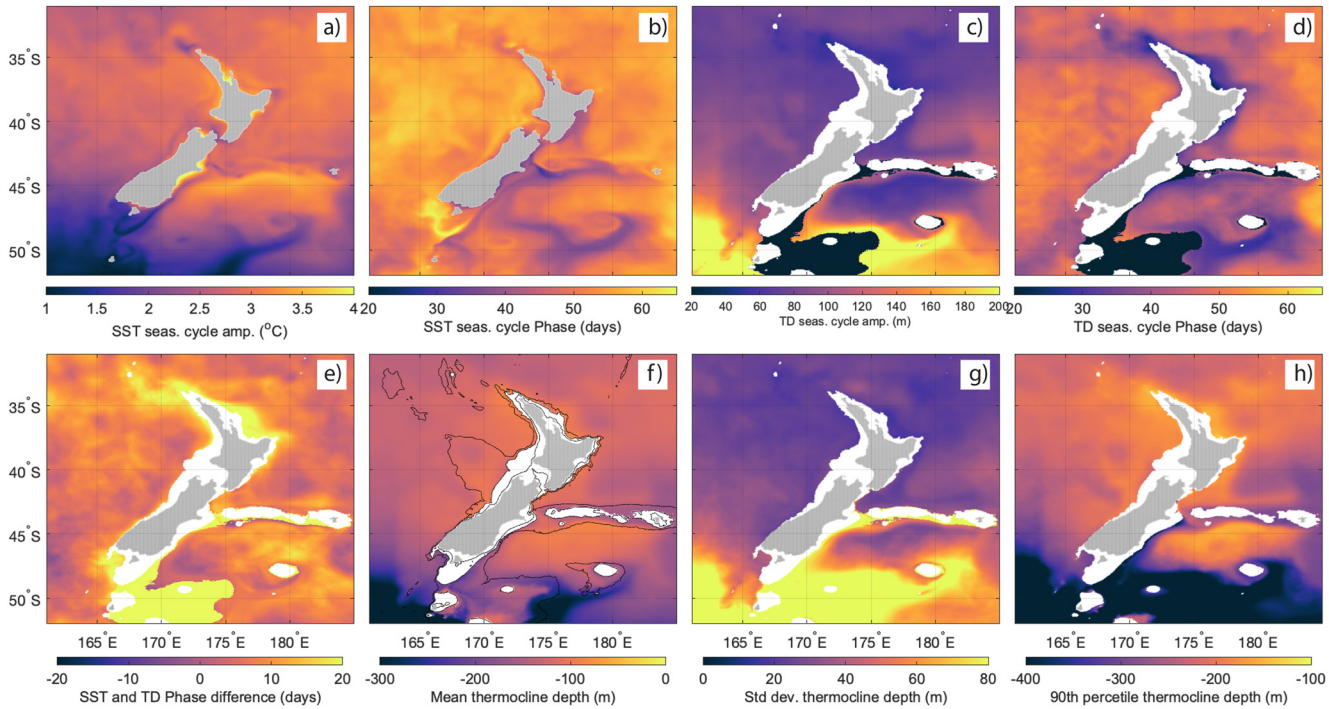


**Figure 9.** Amplitude (a) and phase (b) of the seasonal cycle in Sea Surface Temperature (SST), amplitude (c) and phase (d) of the seasonal cycle in thermocline depth. Phase difference between SST and thermocline depth seasonal cycle (e), mean thermocline depth (f) and standard deviation of thermocline depth (with the seasonal cycle removed, (g)), 90th percentile thermocline depth (used for UOHC calculations, (h)). Mean SST and standard deviation of SST (with the seasonal cycle removed) are shown in Figure 2. Phase is expressed as days to maximum from 1 January.

### 5.2. Thermocline Depth

Estimating thermocline depth (the transition between the warmer upper ocean and the cooler deep water below) is key to estimating UOHC. From the model output, we compute the thermocline depth daily following the variable representative isotherm method, which was shown to be robust and is described in Fiedler (2010). The isotherm representing the thermocline is defined as thermocline temperature $TT = T_{\mathrm{MLD}} - 0.25[T_{\mathrm{MLD}} - T_{400\mathrm{m}}]$, where the temperature at the base of the mixed layer is estimated as $T_{\mathrm{MLD}} = \mathrm{SST} - 0.8$. As such, the thermocline is defined as the layer from the base of the mixed layer to the depth at which temperature has dropped halfway toward the temperature at 400 m, and the thermocline depth is the midpoint of that layer. Note that by definition thermocline depth is not computed where the total water depth is less than 400 m. In the south of the domain where the winter mixed layer depth sometimes exceeds 400 m, the thermocline depth is set to 400 m when this occurs. Tidal variability was removed from the temperature fields before computing the thermocline depth, so the heaving of the isotherms due to internal tides is not captured in the thermocline depth variability presented here.

Both the mean thermocline depth and the variability are considerably greater at higher latitudes (Figures 9f and 9g). The mean thermocline depth is less than 150 m across much of the NZ oceanic region north of the southern tip of the South Island, with a minimum mean of 70 m, and reaches as deep as 388 m in the far south of the model domain (Figure 9f). The amplitude of the thermocline depth seasonal cycle (Figure 9c) is lowest in the EAUC system and to the South of Chatham Rise east of the SC (60–70 m). In the EAUC system, the thermocline shoals 10–20 days before the SST peaks in summer, and the thermocline deepening leads the minimum in SST in winter (Figure 9e). This lead is also evident along the southwestern coastline of the South Island influenced by the STF, and to the south of the Chatham Rise.

The standard deviation of thermocline depth (with the seasonal cycle removed) is less than 40 m over the northern part of the domain, including the entire west coast of NZ, and reaches a maximum standard deviation of 230 m in the far south (Figure 9g). Over the northern region, thermocline depth standard deviation is greatest in the EAUC (30–40 m) and off the east coast of the North Island, offshore of the ECC (35–40 m), compared to ~20–25 m for the rest of the northern region. Off the South Island, thermocline depth varies least in the Bounty Trough



21699291, 2023, 4, Downloaded from https://agupubs.onlinelibrary.wiley.com/doi/10.1029/2022JC018624 by University of New South Wales, Wiley Online Library on [16/10/2023]. See the Terms and Conditions (https://onlinelibrary.wiley.com/terms-and-conditions) on Wiley Online Library for rules of use; OA articles are governed by the applicable Creative Commons License

directly south of the Chatham Rise (standard deviations of 30–45 m) and off the west coast (25–30 m). The region of large thermocline depth variability in the south of the model domain has a water depth of 500–600 m. In the model, from May to July (Austral winter) every year the water column becomes fully mixed and stays that way for winter and spring. At the beginning of Austral summer (October–December) the thermocline then shoals again and ranges between 50 and 150 m for summer and autumn. As such no seasonal cycle is extracted based on a harmonic fit (Figures 9c and 9d) due to the Dirac function nature of the change in thermocline depth due to rapid mixing in winter and shoaling in summer. The thermocline depth standard deviation with the seasonal cycle removed is therefore notably higher than the surrounding regions where a seasonal cycle in thermocline depth can be extracted. The 90th percentile thermocline depth is shown in Figure 9h as this is the depth to which UOHC is computed, for the analysis that follows.

### 5.3. Upper Ocean Heat Content

UOHC is a vital metric to understand heat transfer in and out of the upper ocean and is of key interest for understanding ocean warming (e.g., J. Li et al., 2022b, and others) and the subsurface effects of marine heatwaves (Behrens et al., 2019; Kerry et al., 2022). UOHC quantifies the heat in the upper ocean, and is given by

$$\int_{-z_T}^{0} \rho(z) C_p T(z) dz$$

where $-z_T$ is the depth of the upper layer, $\rho(z)$ is the density at depth $z$, $C_p$ is the specific heat of sea water, and $T(z)$ is the water temperature at depth $z$. To define UOHC we must first define the depth of the upper layer. Bowen et al. (2017) give some justification for integrating over top 250 m for heat budgets in the subtropical NZ region (being the maximum mixed layer depth over the region). However, heat is transported and stored below the mixed layer and we believe thermocline depth is a more appropriate depth. Given that we have 28 yr of 3-dimensional temperature fields from the model, we are able to determine a more appropriate depth limit for the "upper ocean." A comparison of the heat content in the upper 250 m and the upper ocean defined by the 90th percentile thermocline depth (not shown) reveals that using a depth of 250 m means that the mean and variability in UOHC are biased by the latitudinal gradient, while the 90th percentile thermocline depth gives a truer representation of heat content in the "upper ocean." Computing heat content to a depth of 250 m (compared to the 90th percentile thermocline depth) provides an "underestimate" at the higher latitudes (below about 47°S) of up to $1 \times 10^{10}$ Jm$^{-2}$, and an "overestimate" over much of the NZ region covering the northern portion of the South Island and the entire North Island region of 2–6 $\times 10^{9}$ Jm$^{-2}$. We believe that the 90th percentile thermocline depth (which is spatially varying across the domain) is a more appropriate depth to which to compute UOHC, given that the thermocline defines the "upper ocean" in terms of heat content. As such, for this work we define the upper layer as the 90th percentile thermocline depth (Figure 9h). For depths shallower than 400 m (where by definition thermocline depth is not computed) we compute the heat content over the entire water column.

Mean and overall variability of UOHC are presented in Figures 10a and 10b, respectively. UOHC variability is typically greater at inter-annual periods (low-pass filtered at > 450 days) compared to variability at intra-annual periods (band-pass filtered at 60–250 days) over most of the region (comparing Figures 10c and 10d). The difference is most notable for the quiescent region off the west coast of the North Island and the region off the east coast of the South Island, dominated by the coherent SC and the STF and SAF. At intra-annual periods (Figure 10d), near-coast UOHC variability is high off North Cape and in the ECE and WE regions, associated with the mesoscale eddy dominated EAUC/ECC system, as well as off the southwest coast of the South Island, influenced by the STF. Note that the remainder of the total variability (Figure 10b) is dominated by the seasonal cycle.

### 5.4. Co-Variability of Ocean Circulation and UOHC

#### 5.4.1. Boundary Current Transport and Heat Content

Understanding how boundary current transport and UOHC are related can shed light on the mechanisms and the temporal and spatial scales of upper ocean variability. We compute the correlations between volume transport in four major boundary currents and UOHC across the domain, for variability at inter-annual periods (greater than 450 days, Figures 10e–10h) and intra-annual periods (between 60 and 250 days, Figures 10i–10l).

At inter-annual periods, the strength of the EAUC is positively correlated with UOHC (Figure 10e) across most of the NZ region. While this is consistent with the understanding that heat content around NZ is controlled by



21699291, 2023, 4, Downloaded from https://agupubs.onlinelibrary.wiley.com/doi/10.1029/2022JC018624 by University of New South Wales, Wiley Online Library on [16/10/2023]. See the Terms and Conditions (https://onlinelibrary.wiley.com/terms-and-conditions) on Wiley Online Library for rules of use; OA articles are governed by the applicable Creative Commons License

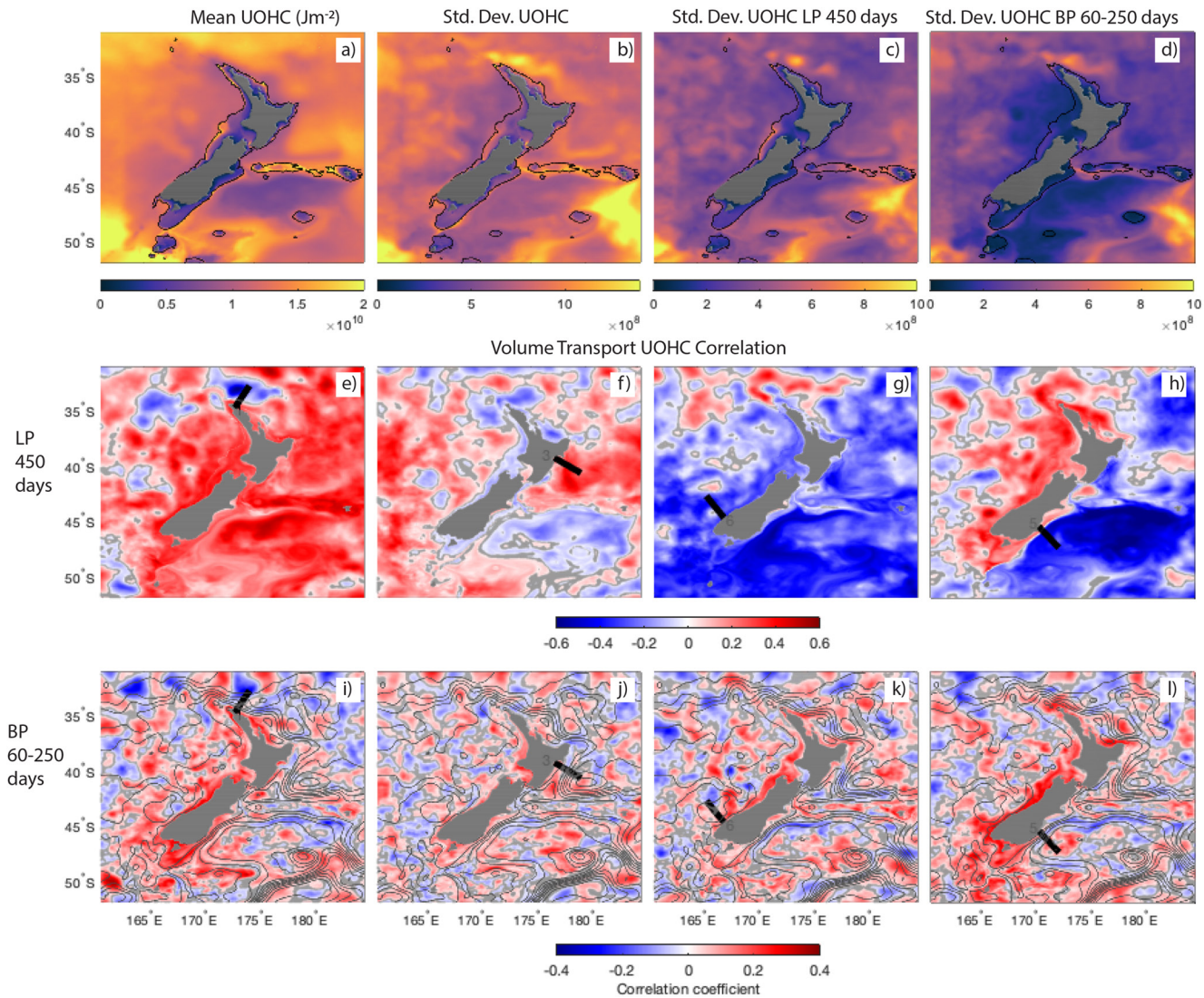


**Figure 10.** Mean Upper ocean heat content (UOHC) above the 90th percentile thermocline depth (a), standard deviation of UOHC (b), standard deviation of UOHC low-pass filtered at 450 days (c), and standard deviation of UOHC band-pass filtered at 60–250 days (d) ($Jm^{-2}$). Correlation of daily volume transport (low-pass filtered at 450 days) through the shown section and daily UOHC (low-pass filtered at 450 days) (e–h). Correlation of daily volume transport (band-pass filtered at 60–250 days) through the shown section and daily UOHC (band-pass filtered at 60–250 days) (i–l). Sections represent (left to right) 1. East Auckland Current, 2. East Cape Current, 3. Fiordland Current, 4. Southland Current (SC). Areas where the correlation is not significant are shaded in gray (*P*-value >0.05). For the correlations, positive volume transport is in the direction of the mean current direction (EAUC, eastward, ECC, southward, Fiorland Current, southward, SC, northward). Current transport is computed within the areas as defined in Figures 4 and 5.

the strength of the EAC eastern extension (Behrens et al., 2019), our result shows that even across the southern region which is not directly influenced by the EAUC system, heat content and EAUC transport are positively correlated. This is likely related to the covariance of SST, subsurface temperature, and steric height around NZ, rather than a direct influence of the EAUC on UOHC through advection. Previous studies have also shown large areas of high correlation at inter-annual time scales (e.g., Bowen et al., 2017). This suggests a large-scale process at play that affects both heat contents over the broad region and transport in the EAC eastern extension/EAUC system at inter-annual periods, such as large-scale oscillations associated with climate modes. This is consistent with Sutton and Bowen (2019) who show significant inter-annual variability in SST is coherent over a large area of ocean north of the STF. A stronger ECC is associated with a warmer upper ocean to the east of the North Island (Figure 10f).

While the focus of this study is not on long-term trends, the results can shed light on warming mechanisms. The warming trends in the southwest Pacific observed by Sutton and Bowen (2019) show the most intense warming in the



21699291, 2023, 4, Downloaded from https://agupubs.onlinelibrary.wiley.com/doi/10.1029/2022JC018624 by University of New South Wales, Wiley Online Library on [16/10/2023]. See the Terms and Conditions (https://onlinelibrary.wiley.com/terms-and-conditions) on Wiley Online Library for rules of use; OA articles are governed by the applicable Creative Commons License

EAC southern extension (their Figure 1) with less warming along the path of the EAC eastern extension and in the northeast of NZ. J. Li et al. (2022b) showed that ocean warming off Tasmania is driven by a poleward shift of the EAC separation latitude and that the warming results from the poleward penetration of the EAC, rather than a strengthening of the current. The pattern observed by Sutton and Bowen (2019) therefore may suggest that warming in the EAUC system may be less extreme as the EAC penetrates further south along the southeastern coast of Australia. However, the role of atmospheric forcing on warming in the Tasman Sea has also been shown to play a significant role, particularly for the west coast of NZ (Bowen et al., 2017). While the effect of long-term changes to the EAC system on warming around NZ requires further investigation, increased understanding of the relationship between heat content around NZ and the strength of its boundary currents provides an important first step toward unraveling this subject.

Cooler upper ocean waters across most of NZ's southern and eastern oceanic region occur when poleward FC transport is high (Figure 10g). SC transport is significantly correlated with warm UOHC across the west and south coasts of NZ (associated with the STF) and a cool upper ocean associated with the SAF (Figure 10h). Indeed a stronger SC is associated with a strong temperature gradient between the STF and the SAF.

At intra-annual timescales (Figures 10i–10l) correlations between current transport and UOHC have more complex spatial structures. The correlation field for EAUC transport and UOHC show an eddy like structure along the path of the EAC eastern extension as it attaches to North Cape. UOHC along the shelf on the west coast of NZ is positively correlated to the strength of the FC and the SC at intra-annual timescales.

### 5.4.2. Co-Variability of SSH and Heat Content

To further investigate the co-variability of the ocean circulation and UOHC we employ Empirical Orthogonal Function (EOF) analysis and Singular Value Decomposition (SVD) to the SSH and UOHC fields. EOF analysis decomposes the field into orthogonal modes of variability (in this case SSH and UOHC separately), while SVD describes the co-variability of two fields (in this case SSH and UOHC). While SSH and UOHC are inevitably correlated, the relationship between SSH and Ocean Heat Content is complex and varies across timescales and regions (Fasullo & Gent, 2017). Exploring their co-variability in this way allows us to detect the most correlated patterns and sheds light on the relationship between the larger-scale ocean circulation (largely described by the SSH field, and easily observed and studied by altimetry) and the corresponding UOHC (which our model allows us to estimate). Similar analysis by J. Li et al. (2022b) revealed that mesoscale eddies drive changes in UOHC in the EAC.

It is clear from performing this analysis over the entire model domain (not shown) that there are two dominant circulation regimes affecting UOHC around NZ: the EAUC system in the north, and the STF-SAF system associated with the SC in the south, while on the west coast of the North island, UOHC and SSH show weak co-variability indicating that surface heat fluxes may dominate rather than large scale ocean circulation. As such, we separate the analysis into the Northern and Southern regions (Figures 11 and 11, respectively). We also analyze a smaller region to focus specifically on the EAUC system (Figure 12), as this region exhibits the highest UOHC variability at intra-annual time scales.

#### *5.4.2.1. Northern Region*

In the northern region (Figure 11), at annual to inter-annual periods (>300 days), SSH and UOHC variability are both dominated by the EAUC mean position (Figures 11e, 11g, 11m, and 11o) with dominant variability at annual and 3-yearly periods (Figures 11u and 11w). This suggests that the strength of the EAUC (the across-current SSH gradient) varies on both seasonal and greater timescales (likely related to large-scale climate modes as suggested above). While the Mode-1 EOF explains 72.9% of the SSH variability (Figure 11e), 96.9% of the UOHC variability is described by the Mode-1 EOF (Figure 11g), and in the SVD 97.5% of the co-variability of SSH and UOHC is described by Mode-1 (Figures 11m and 11o). The Mode-1 spatial structure is representative of the EAUC mean position. The spatial structures of the Mode-1 SVD for SSH (Figure 11m) and UOHC (Figure 11o) are very similar and the mode describes the co-variability of SSH and UOHC with a single temporal expansion function and an explained variability of 97.5%. This is in contrast to the EOF modes which explain the variability of SSH (Figure 11e) and UOHC (Figure 11g) separately. However, of interest are the distinct similarities in spatial structure across the Mode-1 EOFs and the Mode-1 SVD, although for SSH the percentage explained by EOF Mode-1 is lower (72.9%) compared to ∼97% for UOHC variability and SSH-UOHC co-variability.

At intra-annual periods (60–250 days), EOF Mode-1 SSH (Figure 11f) describes an oscillation between the western and eastern sides of the North Island, while the Mode-1 EOF for UOHC (Figure 11h) displays a mesoscale eddy dominated spatial structure (explaining only 4.1% of the variability). The SVD Mode-1 (Figures 11n



21699291, 2023, 4, Downloaded from https://agupubs.onlinelibrary.wiley.com/doi/10.1029/2022JC018624 by University of New South Wales, Wiley Online Library on [16/10/2023]. See the Terms and Conditions (https://onlinelibrary.wiley.com/terms-and-conditions) on Wiley Online Library for rules of use; OA articles are governed by the applicable Creative Commons License

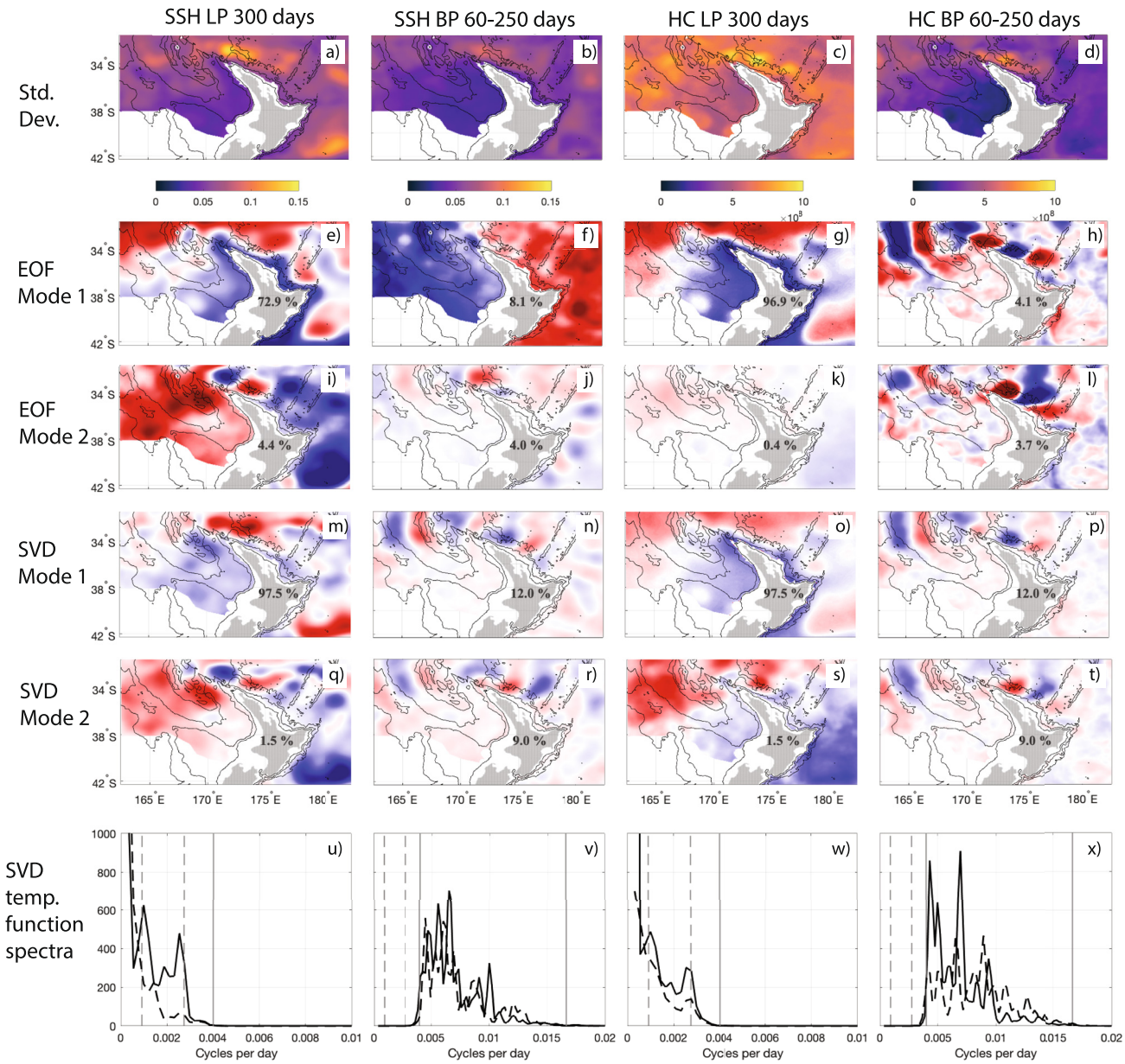


**Figure 11.** Empirical Orthogonal Function (EOF) and Singular Value Decomposition (SVD) analysis over the northern NZ region. Left to right: SSH low-pass filtered at 300 days, band-pass filtered at 60–250 days, UOHC low-pass filtered at 300 days, UOHC band-pass filtered at 60–250 days. Top to bottom: Standard deviation, Mode 1 EOF spatial expansion function, Mode 2 EOF spatial expansion function, Mode 1 SVD spatial expansion function, Mode 2 SVD spatial expansion function, and frequency spectra of the SVD temporal expansion functions. On the frequency spectra the gray dashed lines show the frequencies associated with 3-yearly periods and the annual period, and the gray sold lines show frequencies corresponding to periods of 250 and 60 days.

and 11p) describes 12% of the co-variability between SSH and UOHC and the SVD Mode-2 (Figures 11r and 11t) describes 9%. These percentages are low indicating that no single coherent spatial structure dominates the variability at intra-annual scales. This is due to high eddy variability which is consistent with the lack of significant seasonal differences in volume transport (outside of the monthly standard deviations) over the EAUC. The SVD Mode-1 and Mode-2 spatial patterns (Figures 11n, 11p, 11r, and 11t) show a similar mesoscale eddy dominated spatial structure as the UOHC EOF Mode-1 and Mode-2 (Figures 11h and 11l), with peaks at 230 and 140 days (Figure 11x). These results indicate that UOHC variability at intra-annual timescales is modulated by mesoscale eddies that vary in location; that is, there is no semi-permanent mesoscale eddy structure that explains a high percentage of the SSH and UOHC variability across the northern region.



21699291, 2023, 4, Downloaded from https://agupubs.onlinelibrary.wiley.com/doi/10.1029/2022JC018624 by University of New South Wales, Wiley Online Library on [16/10/2023]. See the Terms and Conditions (https://onlinelibrary.wiley.com/terms-and-conditions) on Wiley Online Library for rules of use; OA articles are governed by the applicable Creative Commons License

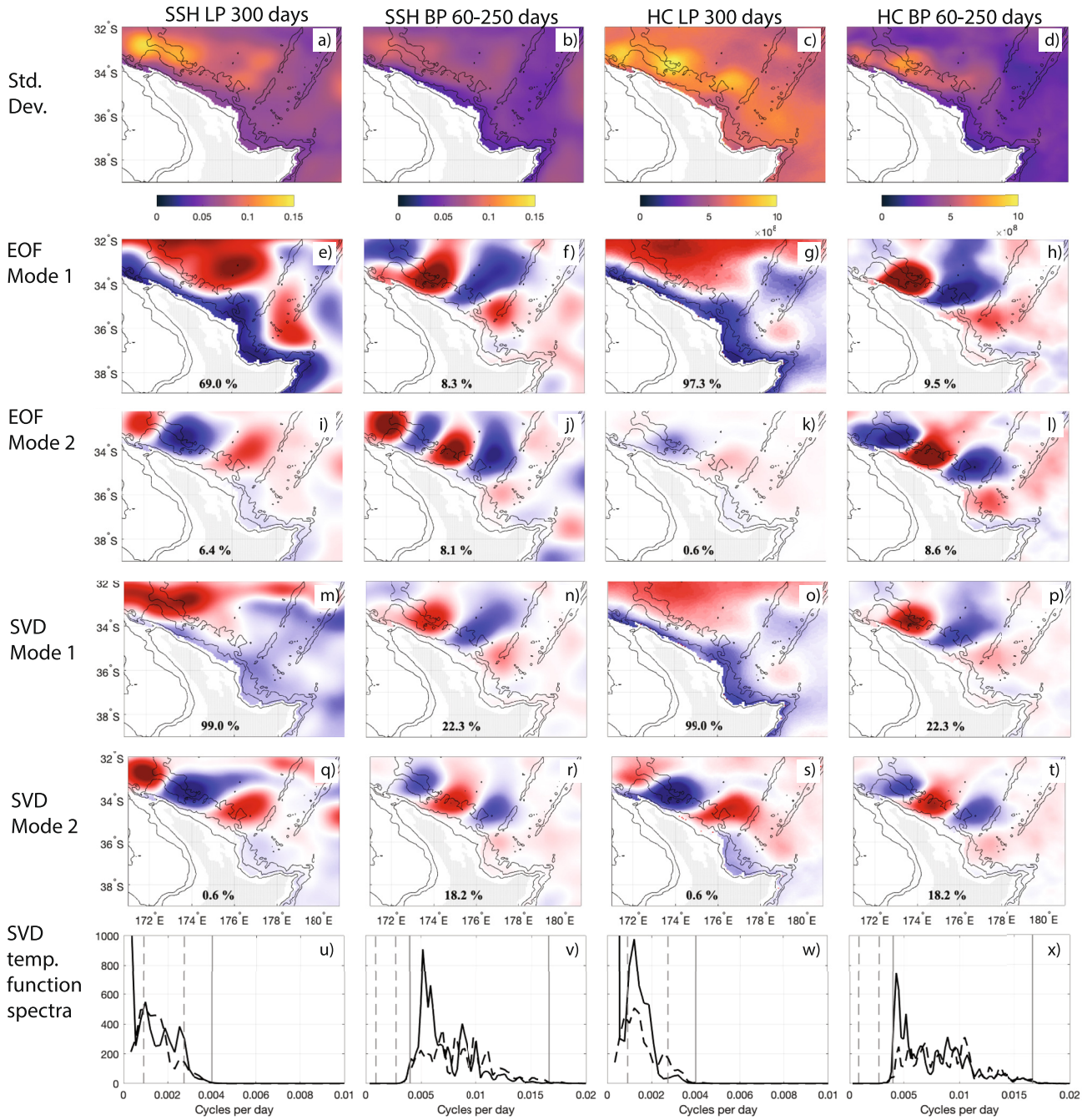


**Figure 12.** Empirical Orthogonal Function (EOF) and Singular Value Decomposition (SVD) analysis over the East Auckland Current region. Left to right: Sea Surface Height (SSH) low-pass filtered at 300 days, band-pass filtered at 60–250 days, upper ocean heat content (UOHC) low-pass filtered at 300 days, UOHC band-pass filtered at 60–250 days. Top to bottom: Standard deviation, Mode 1 EOF spatial expansion function, Mode 2 EOF spatial expansion function, Mode 1 SVD spatial expansion function, Mode 2 SVD spatial expansion function, and frequency spectra of the SVD temporal expansion functions. On the frequency spectra the gray dashed lines show the frequencies associated with 3-yearly periods and the annual period, and the gray sold lines show frequencies corresponding to periods of 250 and 60 days.

However, focusing on the EAUC region alone (Figure 12) we are able to decipher the structure of the mesoscale eddies more clearly. At annual to inter-annual periods SSH and UOHC variability are both dominated by the EAUC mean position (Figures 12e, 12g, 12m, and 12o), and at intra-annual periods variability of SSH and UOHC shows the spatial structure of mesoscale eddies (Figures 12f, 12h, 12j, 12l, 12n, 12p, 12r, and 12t). SVD Mode-1



21699291, 2023, 4, Downloaded from https://agupubs.onlinelibrary.wiley.com/doi/10.1029/2022JC018624 by University of New South Wales, Wiley Online Library on [16/10/2023]. See the Terms and Conditions (https://onlinelibrary.wiley.com/terms-and-conditions) on Wiley Online Library for rules of use; OA articles are governed by the applicable Creative Commons License

at 60–250 days (Figures 12n and 12p) describes an eddy train with the strongest eddy representing separation off North Cape. This structure describes 22.3% of the co-variability between SSH and UOHC and the temporal expansion function has a spectral peak at 190–230 days (Figures 12v and 12x), while the Mode-2 energy is spread evenly across 85–250 days (Figures 12v and 12x) and describes 18.2% of the variability (Figures 12r and 12t). The percentage explained by the SVD Mode-1 and Mode-2 at intra-annual periods is greater when a smaller region focusing on the EAUC is chosen (22.3% and 18.2%, Figures 12n, 12p, 12r, and, 12t), compared to Figures 11n, 11p, 11r, and 11t (12.0% and 9.0%). The spatial structure of the SVD modes and the EOF modes are again similar, indicating that the co-variability of SSH and UOHC over the EAUC region is dominated by the mean position of the EAUC at low frequencies and by mesoscale eddy variability, as displayed by the spatial structure of the modes.

#### *5.4.2.2. Southern Region*

In the Southern region (Figure 13), at annual to inter-annual periods (>300 days), SSH and UOHC vary between the waters to west and to the southeast (the Campbell Plateau) of the South Island associated with the STF and the waters to the east associated with the SAF (the Bounty Trough), Figures 13e, 13g, 13m, and 13o. The Mode-1 EOF of UOHC (Figure 13g) explains 98.7% of the variability while the SVD Mode-1 (Figure 13o) has the same spatial structure and explains 99.8% of the SSH and UOHC co-variability. At intra-annual periods (60–250 days) SSH varies between the western and eastern sides of the South Island (Figure 13f). SSH and UOHC variability show different spatial structures in the EOF Modes at intra-annual periods across the southern region (Figures 13f and 13j for SSH and Figures 13h and 13l for UOHC), and the first two modes only explain 8% of the UOHC variability (Figures 13h and 13l), indicating a lack of coherent circulation features associated with UOHC variability. Indeed, variability in SSH and UOHC at intra-annual timescales is small over the oceanic region east of the South Island, where the circulation is dominated by the highly coherent SC. This is in contrast to the EAUC region, where mesoscale eddies drive UOHC changes at periods of 60–250 days.

## 6. Summary and Conclusions

We use a high-resolution 28 yr ocean hindcast that represents well the ocean circulation around NZ to present a comprehensive characterization of NZ's boundary currents. The model reveals the complex depth structure of the boundary currents and the variability in transport on a range of temporal scales. The model has been comprehensively validated herein and in Azevedo Correia de Souza et al. (2022); the greatest discrepancies with respect to previous work are the modeled estimates of transport in the southern EAUC and the ECC which has been discussed in detail in Section 4.

Model circulation along the north-east coast of NZ is dominated by the EAUC and the ECC, which occur upon reattachment of the EAC eastern extension at the northern tip of NZ. In the model, this eddy-dominated current system exhibits significant strengthening and deepening downstream due to recirculating eddies, with transport increasing from 10 to 38 Sv. On the east coast of the South Island, the SC displays strong seasonality and is highly coherent with mean transport of 9.3 Sv.

We show that inter-annual ocean heat content variability in the NZ region is correlated with the strength of the EAUC. In the EAUC system, UOHC variability is strongly correlated with the mean position of the EAUC at annual to inter-annual time scales, and is dominated by mesoscale eddies at intra-annual time scales. Around the South Island, UOHC varies predominantly at periods greater than 300 days, correlated with variability in the temperature gradient between the STF in the Tasman Sea and the SAF. These results demonstrate for the first time the different temporal and spatial scales of UOHC variability across the NZ region and imply that different mechanisms control heat content across the region.

While various studies exist using observations and/or models to characterize the ocean circulation around NZ, differences in study methodologies, spatial and temporal coverage, and objectives mean that an overall picture of the structure of the boundary currents and their variability has been lacking. Here we use a long-term, realistic, high-resolution ocean hindcast to revisit and characterize the three-dimensional structure and temporal and spatial variability of all NZ's boundary currents in a consistent way. The study puts previous findings into context and identifies gaps in our current knowledge of NZ's circulation and caveats in observations. The characterization provides a useful review to guide future research goals, including observational campaigns, across the region.

The high-resolution model allows the complex coastal boundary currents and temperature variability to be resolved while the spatial extent of the domain allows the study of large scale relationships between current



21699291, 2023, 4, Downloaded from https://agupubs.onlinelibrary.wiley.com/doi/10.1029/2022JC018624 by University of New South Wales, Wiley Online Library on [16/10/2023]. See the Terms and Conditions (https://onlinelibrary.wiley.com/terms-and-conditions) on Wiley Online Library for rules of use; OA articles are governed by the applicable Creative Commons License

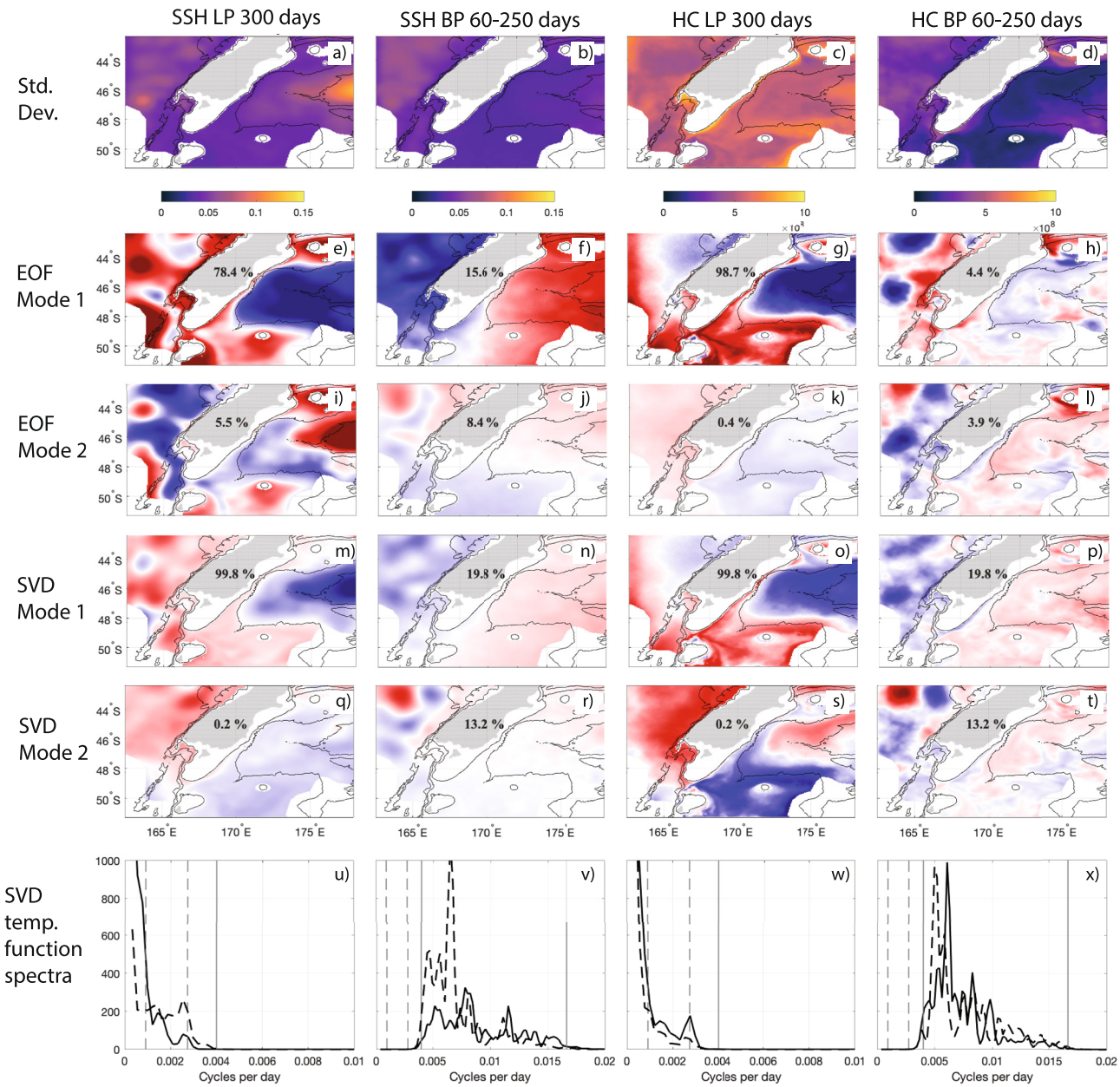


**Figure 13.** Empirical Orthogonal Function (EOF) and Singular Value Decomposition (SVD) analysis over the southern NZ region. Left to right: Sea Surface Height (SSH) low-pass filtered at 300 days, band-pass filtered at 60–250 days, upper ocean heat content (UOHC) low-pass filtered at 300 days, UOHC band-pass filtered at 60–250 days. Top to bottom: Standard deviation, Mode 1 EOF spatial expansion function, Mode 2 EOF spatial expansion function, Mode 1 SVD spatial expansion function, Mode 2 SVD spatial expansion function, and frequency spectra of the SVD temporal expansion functions. On the frequency spectra the gray dashed lines show the frequencies associated with 3-yearly periods and the annual period, and the gray sold lines show frequencies corresponding to periods of 250 and 60 days.

transport and ocean heat content. Revealing the spatial structures of variability of UOHC at both intra-annual and annual to inter-annual timescales provides invaluable context for understanding the drivers of ocean heat content variability. This understanding is a crucial step toward predicting ocean heat content extremes. Furthermore, this characterization provides a basis for understanding how climate change may impact NZ's oceans, with both large-scale adjustments and eddies impacting UOHC. Significantly, recent studies have highlighted the importance of eddies in ocean warming hotspots (J. Li et al., 2022a; Yang, 2022).



21699291, 2023, 4, Downloaded from https://agupubs.onlinelibrary.wiley.com/doi/10.1029/2022JC018624 by University of New South Wales, Wiley Online Library on [16/10/2023]. See the Terms and Conditions (https://onlinelibrary.wiley.com/terms-and-conditions) on Wiley Online Library for rules of use; OA articles are governed by the applicable Creative Commons License

## Data Availability Statement

The model data is available at Azevedo Correia de Souza (2022), https://doi.org/10.5281/zenodo.5895265.

**Acknowledgments**
This research and C.K. were supported by the Moana Project (www.moanaproject.org) funded by the New Zealand Ministry of Business Innovation and Employment, contract number METO1801 to M.R. Open access publishing facilitated by University of New South Wales, as part of the Wiley - University of New South Wales agreement via the Council of Australian University Librarians.

## References

Andres, M., Mensah, V., Jan, S., Chang, M., Yang, Y., Lee, C. M., et al. (2017). Downstream evolution of the Kuroshio's time-varying transport and velocity structure. *Journal of Geophysical Research: Oceans*, *122*(5), 3519–3542. https://doi.org/10.1002/2016jc012519

Archer, M., Roughan, M., Keating, S., & Schaeffer, A. (2017). On the variability of the East Australian Current: Jet structure, meandering, and influence on shelf circulation. *Journal of Geophysical Research: Oceans*, *122*(11), 1–18. https://doi.org/10.1002/2017jc013097

Azevedo Correia de Souza, J. M. (2022). Moana Ocean Hindcast. Zenodo. https://doi.org/10.5281/zenodo.5895265

Azevedo Correia de Souza, J. M., Suanda, S. H., Couto, P. P., Smith, R. O., Kerry, C., & Roughan, M. (2022). Moana Ocean Hindcast—A 25+ yr simulation for New Zealand Waters using the ROMS v3.9 model. *EGUsphere*, 1–34. https://doi.org/10.5194/egusphere-2022-41

Ballarotta, M., Ubelmann, C., Pujol, M. I., Taburet, G., Fournier, F., Legeais, J. F., et al. (2019). On the resolutions of ocean altimetry maps. *Ocean Science*, *15*(4), 1091–1109. https://doi.org/10.5194/os-15-1091-2019

Baxter, T. (2022). *The impact of tidal forcing on the oceanography of the northern continental shelf of New Zealand (Unpublished doctoral dissertation)*. University of Otago.

Behrens, E., Fernandez, D., & Sutton, P. J. (2019). Meridional oceanic heat transport influences marine heatwaves in the Tasman Sea on interannual to decadal timescales. *Frontiers in Marine Science*, *6*, 228. https://doi.org/10.3389/fmars.2019.00228

Bostock, H., Opdyke, B., Gagan, M., Kiss, A., & Fifield, L. K. (2006). Glacial/interglacial changes in the East Australian Current. *Climate Dynamics*, *26*(6), 645–659. https://doi.org/10.1007/s00382-005-0103-7

Bowen, M., Markham, J., Sutton, P. J., Zhang, X., Wu, Q., Shears, N., & Fernandez, D. (2017). Interannual variability of Sea Surface Temperature in the southwest Pacific and the role of ocean dynamics. *Journal of Climate*, *30*(18), 7481–7492. https://doi.org/10.1175/jcli-d-16-0852.1

Bowen, M., Sutton, P. J., & Roemmich, D. (2014). Estimating mean dynamic topography in boundary currents and the use of Argo trajectories. *Journal of Geophysical Research: Oceans*, *119*(12), 8422–8437. https://doi.org/10.1002/2014JC010281

Bowman, M. J., Kibblewhite, A. C., Murtagh, R. A., Chiswell, S. M., & Sanderson, B. G. (1983). Circulation and mixing in greater Cook Strait, New Zealand. *Oceanologica Acta*, *6*(4), 383–391.

Bull, C. Y. S., Kiss, A. E., Van Sebille, E., Jourdain, N. C., & England, M. H. (2018). The role of the New Zealand Plateau in the Tasman Sea Circulation and Separation of the East Australian Current. *Journal of Geophysical Research: Oceans*, *123*(2), 1457–1470. https://doi.org/10.1002/2017jc013412

Cahill, M. L., Middleton, J. H., & Stanton, B. R. (1991). Coastal-trapped waves on the west coast of South Island, New Zealand. *Journal of Physical Oceanography*, *21*(4), 541–557. https://doi.org/10.1175/1520-0485(1991)021<0541:ctwotw>2.0.co;2

Cetina Heredia, P., Roughan, M., Van Sebille, E., & Coleman, M. (2014). Long-term trends in the East Australian Current separation latitude and eddy driven transport. *Journal of Geophysical Research: Oceans*, *119*(7), 4351–4366. https://doi.org/10.1002/2014JC010071

Chandler, M., Bowen, M., & Owain Smith, R. (2019). The Fiordland Current, southwest New Zealand: Mean, variability, and trends. *New Zealand Journal of Marine and Freshwater Research.*, *55*(1), 156–176. https://doi.org/10.1080/00288330.2019.1629467

Chiswell, S. M. (1996). Variability in the Southland Current, New Zealand. *New Zealand Journal of Marine and Freshwater Research*, *30*(1), 1–17. https://doi.org/10.1080/00288330.1996.9516693

Chiswell, S. M. (2000). The Wairarapa coastal current. *New Zealand Journal of Marine and Freshwater Research*, *34*(2), 303–315. https://doi.org/10.1080/00288330.2000.9516934

Chiswell, S. M. (2001). Eddy energetics in the subtropical front over the Chatham Rise, New Zealand. *New Zealand Journal of Marine and Freshwater Research*, *35*(1), 1–15. https://doi.org/10.1080/00288330.2001.9516975

Chiswell, S. M. (2003). Circulation within the Wairarapa Eddy, New Zealand. *New Zealand Journal of Marine and Freshwater Research*, *37*(4), 691–704. https://doi.org/10.1080/00288330.2003.9517199

Chiswell, S. M. (2005). Mean and variability in the Wairarapa and Hikurangi eddies, New Zealand. *New Zealand Journal of Marine and Freshwater Research*, *39*(1), 121–134. https://doi.org/10.1080/00288330.2005.9517295

Chiswell, S. M., Bostock, H. C., Sutton, P. J., & Williams, M. J. M. (2015). Physical oceanography of the deep seas around New Zealand: A review. *New Zealand Journal of Marine and Freshwater Research*, *49*(2), 286–317. https://doi.org/10.1080/00288330.2014.992918

Chiswell, S. M., & Roemmich, D. (1998). The East Cape Current and two eddies: A mechanism for larval retention? *New Zealand Journal of Marine and Freshwater Research*, *32*(3), 385–397. https://doi.org/10.1080/00288330.1998.9516833

Ducet, N., Le Traon, P. Y., & Reverdin, G. (2000). Global high-resolution mapping of ocean circulation from TOPEX/Poseidon and ERS-1 and -2. *Journal of Geophysical Research*, *105*(C8), 19477–19498. https://doi.org/10.1029/2000JC900063

Egbert, G. D., & Erofeeva, S. Y. (2002). Efficient inverse modeling of barotropic ocean tides. *Journal of Atmospheric and Oceanic Technology*, *19*(2), 183–204. https://doi.org/10.1175/1520-0426(2002)019<0183:eimobo>2.0.co;2

Elzahaby, Y., Schaeffer, A., Roughan, M., & Delaux, S. (2021). Oceanic circulation drives the deepest and longest marine heatwaves in the East Australian Current System. *Geophysical Research Letters*, *48*(17). https://doi.org/10.1029/2021GL094785

Fairall, C. W., Bradley, E. F., Rogers, D. P., Edson, J. B., & Young, G. S. (1996). Bulk parameterization of air-sea fluxes for tropical ocean-global atmosphere Coupled-Ocean Atmosphere Response Experiment. *Journal of Geophysical Research*, *101*(C2), 3747–3764. https://doi.org/10.1029/95jc03205

Fasullo, J. T., & Gent, P. R. (2017). On the relationship between regional ocean heat content and sea surface height. *Journal of Climate*, *30*(22), 9195–9211. https://doi.org/10.1175/JCLI-D-16-0920.1

Fernandez, D., Bowen, M., & Carter, L. (2014). Intensification and variability of the confluence of subtropical and subantarctic boundary currents east of New Zealand. *Journal of Geophysical Research: Oceans*, *119*(2), 1146–1160. https://doi.org/10.1002/2013jc009153

Fernandez, D., Bowen, M., & Sutton, P. (2018). Variability, coherence and forcing mechanisms in the New Zealand ocean boundary currents. *Progress in Oceanography*, *165*, 168–188. https://doi.org/10.1016/j.pocean.2018.06.002

Fiedler, P. C. (2010). Comparison of objective descriptions of the thermocline. *Limnology and Oceanography: Methods*, *8*(6), 313–325. https://doi.org/10.4319/lom.2010.8.313

Ganachaud, A., Cravatte, S., Melet, A., Schiller, A., Holbrook, N., Sloyan, B., et al. (2014). The southwest Pacific Ocean circulation and climate experiment (SPICE). *Journal of Geophysical Research: Oceans*, *119*(11), 7660–7686. https://doi.org/10.1002/2013jc009678

Greig, M. J., & Gilmour, A. E. (1992). Flow through the Mernoo Saddle, New Zealand. *New Zealand Journal of Marine and Freshwater Research*, *26*(2), 155–165. https://doi.org/10.1080/00288330.1992.9516510



21699291, 2023, 4, Downloaded from https://agupubs.onlinelibrary.wiley.com/doi/10.1029/2022JC018624 by University of New South Wales, Wiley Online Library on [16/10/2023]. See the Terms and Conditions (https://onlinelibrary.wiley.com/terms-and-conditions) on Wiley Online Library for rules of use; OA articles are governed by the applicable Creative Commons License

Hadfield, M. G., & Stevens, C. L. (2020). A modeling synthesis of the volume flux through Cook Strait. *New Zealand Journal of Marine and Freshwater Research*, *1–29*(1), 65–93. https://doi.org/10.1080/00288330.2020.1784963

Heath, R. A. (1971). Hydrology and circulation in central and southern Cook Strait, New Zealand. *New Zealand Journal of Marine and Freshwater Research*, *5*(1), 178–199. https://doi.org/10.1080/00288330.1971.9515375

Heath, R. A. (1982). What drives the mean circulation on the New Zealand west coast continental shelf? *New Zealand Journal of Marine and Freshwater Research*, *16*(2), 215–226. https://doi.org/10.1080/00288330.1982.9515964

Heath, R. A. (1985). A review of the physical oceanography of the seas around New Zealand—1982. *New Zealand Journal of Marine & Freshwater Research*, *19*(1), 79–124. https://doi.org/10.1080/00288330.1985.9516077

Hill, K., Rintoul, S., Coleman, R., & Ridgway, K. (2008). Wind forced low-frequency variability of the East Australia Current. *Geophysical Research Letters*, *35*(8), L08602. https://doi.org/10.1029/2007gl032912

Hobday, A. J., Alexander, L. V., Perkins, S. E., Smale, D. A., Straub, S. C., Oliver, E. C., et al. (2016). A hierarchical approach to defining marine heatwaves. *Progress in Oceanography*, *141*, 227–238. https://doi.org/10.1016/j.pocean.2015.12.014

Hopkins, J., Shaw, A., & Challenor, P. (2010). The Southland Front, New Zealand: Variability and ENSO correlations. *Continental Shelf Research*, *30*(14), 1535–1548. https://doi.org/10.1016/j.csr.2010.05.016

Huang, B., Liu, C., Banzon, V., Freeman, E., Graham, G., Hankins, B., et al. (2021). Improvements of the Daily Optimum Interpolation Sea Surface Temperature (DOISST) Version 2.1. *Journal of Climate*, *34*(8), 2923–2939. https://doi.org/10.1175/JCLI-D-20-0166.1

Janekovic, I., & Powell, B. (2012). Analysis of imposing tidal dynamics to nested numerical models. *Continental Shelf Research*, *34*, 30–40. https://doi.org/10.1016/j.csr.2011.11.017

Kerry, C., & Roughan, M. (2020). Downstream evolution of the East Australian Current System: Mean flow, seasonal, and intra-annual variability. *Journal of Geophysical Research: Oceans*. e2019JC015227. https://doi.org/10.1029/2019JC015227

Kerry, C., Roughan, M., & Azevedo Correia de Souza, J. M. (2022). Drivers of upper ocean heat content extremes around New Zealand revealed by adjoint sensitivity analysis. *Frontiers in Climate*, *4*, 205. https://doi.org/10.3389/fclim.2022.980990

Li, J., Roughan, M., & Kerry, C. (2021). Dynamics of interannual eddy kinetic energy modulations in a Western Boundary Current. *Geophysical Research Letters*, *48*(19), e2021GL094115. https://doi.org/10.1029/2021gl094115

Li, J., Roughan, M., & Kerry, C. (2022a). Drivers of ocean warming in the Western Boundary Currents of the Southern Hemisphere. *Nature Climate Change*, *12*(10), 901–909. https://doi.org/10.1038/s41558-022-01473-8

Li, J., Roughan, M., & Kerry, C. (2022b). Variability and drivers of ocean temperature extremes in a warming Western Boundary Current. *Journal of Climate*, *35*(3), 1097–1111. https://doi.org/10.1175/JCLI-D-21-0622.1

Li, Z., Holbrook, N. J., Zhang, X., Oliver, E. C. J., & Cougnon, E. A. (2020). Remote forcing of Tasman Sea marine heatwaves. *Journal of Climate*, *33*(12), 5337–5354. https://doi.org/10.1175/JCLI-D-19-0641.1

Morris, M., Stanton, B. R., & Neil, H. (2001). Subantarctic oceanography around New Zealand: Preliminary results from an ongoing survey. *New Zealand Journal of Marine and Freshwater Research*, *35*(3), 499–519. https://doi.org/10.1080/00288330.2001.9517018

Oke, P. R., Pilo, G. S., Ridgway, K. R., Kiss, A., & Rykova, T. (2019). A search for the Tasman Front. *Journal of Marine Systems*, *199*, 103217. https://doi.org/10.1016/j.jmarsys.2019.103217

Oke, P. R., Roughan, M., Cetina-Heredia, P., Pilo, G. S., Ridgway, K. R., Rykova, T., et al. (2019). Revisiting the circulation of the East Australian Current: Its path, separation, and eddy field. *Progress in Oceanography*, *176*, 102139. https://doi.org/10.1016/j.pocean.2019.102139

Oliver, E. C. J., & Holbrook, N. J. (2014). Extending our understanding of South Pacific gyre "spin-up": Modeling the East Australian Current in a future climate. *Journal of Geophysical Research: Oceans*, *119*(5), 2788–2805. https://doi.org/10.1002/2013jc009591

Orsi, A. H., Whitworth, T., III, & Nowlin, W. D., Jr. (1995). On the meridional extent and fronts of the Antarctic Circumpolar Current. *Deep-Sea Research Part I Oceanographic Research Papers*, *42*(5), 641–673. https://doi.org/10.1016/0967-0637(95)00021-w

Qiu, B., & Chen, S. (2004). Seasonal modulations in the eddy field of the South Pacific Ocean. *Journal of Physical Oceanography.*, *34*(7), 1515–1527. https://doi.org/10.1175/1520-0485(2004)034<1515:smitef>2.0.co;2

Reid, J. L. (1986). On the total geostrophic circulation of the South Pacific Ocean: Flow patterns, tracers, and transports. *Progress in Oceanography*, *16*(1), 1–61. https://doi.org/10.1016/0079-6611(86)90036-4

Ridgway, K., & Dunn, J. (2003). Mesoscale structure of the mean East Australian Current system and its relationship with topography. *Progress in Oceanography*, *56*(2), 189–222. https://doi.org/10.1016/s0079-6611(03)00004-1

Ridgway, K., & Godfrey, J. (1994). Mass and heat budgets in the East Australian Current: A direct approach. *Journal of Geophysical Research*, *99*(C2), 3231–3248. https://doi.org/10.1029/93jc02255

Ridgway, K., & Godfrey, J. (1997). Seasonal cycle of the East Australian Current. *Journal of Geophysical Research*, *102*(C10), 22921–22936. https://doi.org/10.1029/97jc00227

Roemmich, D., & Sutton, P. J. (1998). The mean and variability of ocean circulation past northern New Zealand: Determining the representativeness of hydrographic climatologies. *Journal of Geophysical Research*, *103*(C6), 13041–13054. https://doi.org/10.1029/98jc00583

Roughan, M., & Middleton, J. H. (2004). On the East Australian Current: Variability, encroachment, and upwelling. *Journal of Geophysical Research*, *109*(C7), C07003. https://doi.org/10.1029/2003jc001833

Santana, R., Suanda, S. H., McDonald, H., & 'Callaghan, J. O. (2021). Mesoscale and wind-driven variability in the East Auckland Current. *Scientific Reports*, *11*(1), 9764. https://doi.org/10.1038/s41598-021-89222-3

Saunders, P. M., Coward, A. C., & de Cuevas, B. A. (1999). Circulation of the Pacific Ocean seen in a global ocean model: Ocean Circulation and Climate Advanced Modeling project (OCCAM). *Journal of Geophysical Research*, *104*(C8), 18281–18299. https://doi.org/10.1029/1999jc900091

Shaw, A., & Vennell, R. (2000). Variability of water masses through the Mernoo saddle, South Island, New Zealand. *New Zealand Journal of Marine and Freshwater Research*, *34*(1), 103–116. https://doi.org/10.1080/00288330.2000.9516918

Shchepetkin, A. F., & McWilliams, J. C. (2005). The Regional Oceanic Modeling System (ROMS): A split-explicit, free-surface, topography-following-coordinate oceanic model. *Ocean Modeling*, *9*(4), 347–404. https://doi.org/10.1016/j.ocemod.2004.08.002

Sloyan, B. M., Ridgway, K. R., & Cowley, R. (2016). The East Australian Current and property transport at 27°S from 2012 to 2013. *Journal of Physical Oceanography*, *46*(3), 993–1008. https://doi.org/10.1175/jpo-d-15-0052.1

Smith, R. O., Vennell, R., Bostock, H. C., & Williams, M. J. (2013). Interaction of the subtropical front with topography around Southern New Zealand. *Deep Sea Research Part I: Oceanographic Research Papers*, *76*, 13–26. https://doi.org/10.1016/j.dsr.2013.02.007

Sokolov, S., & Rintoul, S. R. (2009). Circumpolar structure and distribution of the Antarctic Circumpolar Current fronts: 2. Variability and relationship to sea surface height. *Journal of Geophysical Research*, *114*(C11), C11019. https://doi.org/10.1029/2008jc005248

Stanton, B. R. (1976). Circulation and hydrology off the west coast of the South Island, New Zealand. *New Zealand Journal of Marine and Freshwater Research*, *10*(3), 445–467. https://doi.org/10.1080/00288330.1976.9515629



21699291, 2023, 4, Downloaded from https://agupubs.onlinelibrary.wiley.com/doi/10.1029/2022JC018624 by University of New South Wales, Wiley Online Library on [16/10/2023]. See the Terms and Conditions (https://onlinelibrary.wiley.com/terms-and-conditions) on Wiley Online Library for rules of use; OA articles are governed by the applicable Creative Commons License

Stanton, B. R. (1995). Sea level variability on the West Coast of New Zealand. *Journal of Physical Oceanography*, *25*(6), 1265–1272. https://doi.org/10.1175/1520-0485(1995)025⟨1265:SLVOTW⟩2.0.CO;2

Stanton, B. R., & Morris, M. Y. (2004). Direct velocity measurements in the Subantarctic Front and over Campbell Plateau, southeast of New Zealand. *Journal of Geophysical Research: Oceans*, *109*(C1), C01028. https://doi.org/10.1029/2002jc001339

Stanton, B. R., & Sutton, P. H. (2003). Velocity measurements in the East Auckland Current north-east of North Cape, New Zealand. *New Zealand Journal of Marine and Freshwater Research*, *37*(1), 195–204. https://doi.org/10.1080/00288330.2003.9517157

Stanton, B. R., Sutton, P. J., & Chiswell, S. M. (1997). The East Auckland Current, 1994–1995. *New Zealand Journal of Marine and Freshwater Research*, *31*(4), 537–549. https://doi.org/10.1080/00288330.1997.9516787

Stevens, C. L. (2014). Residual flows in Cook Strait, a large tidally dominated strait. *Journal of Physical Oceanography*, *44*(6), 1654–1670. https://doi.org/10.1175/jpo-d-13-041.1

Stevens, C. L., O'Callaghan, J. M., Chiswell, S. M., & Hadfield, M. G. (2019). Physical oceanography of New Zealand/Aotearoa shelf seas—A review. *New Zealand Journal of Marine and Freshwater Research*, *0*(0), 1–40. https://doi.org/10.1080/00288330.2019.1588746

Stramma, L., Peterson, R. G., & Tomczak, M. (1995). The South Pacific Current. *Journal of Physical Oceanography*, *25*(1), 77–91. https://doi.org/10.1175/1520-0485(1995)025⟨0077:TSPC⟩2.0.CO;2

Suthers, I. M., Everett, J. D., Roughan, M., Young, J. W., Oke, P. R., Condie, S. A., et al. (2011). The strengthening of the East Australian Current, its eddies and biological effects—An introduction and overview. *Deep-Sea Research II*, *58*(5), 538–546. https://doi.org/10.1016/j.dsr2.2010.09.029

Sutton, P. J. (2001). Detailed structure of the subtropical front over Chatham Rise, east of New Zealand. *Journal of Geophysical Research*, *106*(C12), 31045–31056. https://doi.org/10.1029/2000jc000562

Sutton, P. J. (2003). The Southland Current: A subantarctic current. *New Zealand Journal of Marine and Freshwater Research*, *37*(3), 645–652. https://doi.org/10.1080/00288330.2003.9517195

Sutton, P. J., & Bowen, M. (2011). Currents off the west coast of Northland, New Zealand. *New Zealand Journal of Marine and Freshwater Research*, *45*(4), 609–624. https://doi.org/10.1080/00288330.2011.569729

Sutton, P. J., & Bowen, M. (2014). Flows in the Tasman Front south of Norfolk Island. *Journal of Geophysical Research: Oceans*, *119*(5), 3041–3053. https://doi.org/10.1002/2013JC009543

Sutton, P. J., & Bowen, M. (2019). Ocean temperature change around New Zealand over the last 36 yr. *New Zealand Journal of Marine and Freshwater Research*, *53*(3), 305–326. https://doi.org/10.1080/00288330.2018.1562945

Sutton, P. J., & Chereskin, T. K. (2002). Absolute geostrophic currents in the East Auckland Current region. *New Zealand Journal of Marine & Freshwater Research*, *36*(4), 751–762. https://doi.org/10.1080/00288330.2002.9517128

Tilburg, C. E., Hurlburt, H. E., O'Brien, J. J., & Shriver, J. F. (2001). The dynamics of the East Australian Current system: The Tasman Front, the East Auckland Current, and the East Cape Current. *Journal of Physical Oceanography*, *31*(10), 2917–2943. https://doi.org/10.1175/1520-0485(2001)031<2917:tdotea>2.0.co;2

Tilburg, C. E., Hurlburt, H. E., O'Brien, J. J., & Shriver, J. F. (2002). Remote topographic forcing of a Baroclinic Western Boundary Current: An explanation for the Southland Current and the pathway of the subtropical front east of New Zealand. *Journal of Physical Oceanography*, *32*(11), 3216–3232. https://doi.org/10.1175/1520-0485(2002)032⟨3216:RTFOAB⟩2.0.CO;2

Tomczak, M., & Godfrey, J. S. (1994). *Regional oceanography: An introduction (No. 422)*. Pergamon.

Walters, R. A., Gillibrand, P. A., Bell, R. G., & Lane, E. M. (2010). A study of tides and currents in Cook Strait, New Zealand. *Ocean Dynamics*, *60*(6), 1559–1580. https://doi.org/10.1007/s10236-010-0353-8

Wilkin, J. L., & Zhang, W. G. (2007). Modes of Mesoscale Sea surface height and temperature variability in the East Australian Current. *Journal of Geophysical Research*, *112*(C1), C01013. https://doi.org/10.1029/2006jc003590

Yang, H. (2022). Warming hotspots induced by more eddies. *Nature Climate Change*, *12*(10), 889–890. https://doi.org/10.1038/s41558-022-01488-1

Ypma, S. L., van Sebille, E., Kiss, A. E., & Spence, P. (2016). The separation of the East Australian Current: A Lagrangian approach to potential vorticity and upstream control. *Journal of Geophysical Research: Oceans*, *121*(1), 758–774. https://doi.org/10.1002/2015jc011133



21699291, 2023, 4, Downloaded from https://agupubs.onlinelibrary.wiley.com/doi/10.1029/2022JC018624 by University of New South Wales, Wiley Online Library on [16/10/2023]. See the Terms and Conditions (https://onlinelibrary.wiley.com/terms-and-conditions) on Wiley Online Library for rules of use; OA articles are governed by the applicable Creative Commons License